# Incorporating the impact of floating piles in estimation of large-scale subsidence



Citation for the original published paper (version of record):
Wikby, P., Abed, A., Karstunen, M. et al (2026). Incorporating the impact of floating piles in estimation of large-scale subsidence. Computers and Geotechnics, 200.
http://dx.doi.org/10.1016/j.compgeo.2026.108410



(article starts on next page)

Computers and Geotechnics 200 (2026) 108410

Contents lists available at ScienceDirect

Computers and Geotechnics

journal homepage: www.elsevier.com/locate/compgeo

Research paper

# Incorporating the impact of floating piles in estimation of large-scale subsidence

Pierre Wikby [a,b,*], Ayman Abed [a], Minna Karstunen [a], Jelke Dijkstra [a]

[a] Department of Architecture and Civil Engineering, Chalmers University of Technology, Sweden
[b] COWI AB, Sweden

ARTICLE INFO

*Keywords:*
Floating piles
Interaction level
Modification factors
Settlements
Time-dependence
Building damage

ABSTRACT

The current methods to predict subsidence due to underdrainage on a large-scale, and the consequent damage, tend to neglect the soil–structure interaction, potentially overestimating damage to piled buildings. This paper investigates the settlements of floating piles caused by underdrainage and proposes time-dependent modification factors for greenfield settlements for building damage predictions at large scale. The modification factors are derived from a series of finite element analyses that consider a floating pile in soft clay in which the thickness of the clay layer, the drawdown scenarios, and the load of the pile head are systematically varied. The results are compiled in normalised graphs of the interaction levels evaluated and the settlement modification factors derived for use in models to predict building damage at large-scale. In contrast to greenfield predictions, the long-term subsidence of piled buildings is significantly reduced (approximately 20%). Additionally, long-term interaction levels are shown to be well-approximated by the simple methods more commonly used in industry (2/3-depth and $\alpha$-methods). The magnitude of pile head displacements is significantly influenced by the drawdown and the clay thickness. Finally, the viability of the method is demonstrated for the assessment of building damage in central Gothenburg. The new time-dependent modification factors for piled buildings are shown to be more significant for low-level damage predictions, where for one scenario, the new damage classification led to a reduction in assessed damage for ca. 23% of the piled buildings.

## 1. Introduction

Subsidence due to pore pressure reduction in the draining layers below soft clay deposits can cause damage to buildings and infrastructure, leading to significant societal and economic costs, especially in coastal regions with large urban areas. This so-called underdrainage can result from the extraction of groundwater from the aquifer below the soft soil, e.g. Venice (Teatini et al., 2006), Mexico City (Rodríguez-Rebolledo et al., 2015) and Bangkok (Phien-wej et al., 2006). Furthermore, drawdown can be caused by leakage into tunnels and other underground infrastructure in confined aquifers (e.g. Karlsrud and Sander, 1978; Shen and Xu, 2011; Sundell et al., 2019; Merisalu et al., 2023; Haaf et al., 2024). Modelling the impact of subsidence on a regional scale requires models that balance accuracy with computational efficiency. Often, hydrogeological models are coupled with simplified mechanical models for the prediction of final settlements (Hoffmann et al., 2003; Teatini et al., 2006; Shen and Xu, 2011; Ye et al., 2016; Sundell et al., 2019) or settlements as a function of time (Zhang et al., 2015; Lizárraga and Buscarnera, 2020; Haaf et al., 2024). More recently, data-driven approaches have been proposed, e.g. those developed starting from high-fidelity numerical models (Haaf et al., 2024). So far, a major limitation of large-scale models is the absence of incorporation of the soil–structure interaction between the buildings, their foundation and the soft clay. Consequently, the subsidence models tend to overpredict the magnitude of the total and differential settlements of the affected buildings. This is further exacerbated by foundation solutions that are non-homogeneous with different foundation depths or types, leading to an increase in differential settlements (Phien-wej et al., 2006; Rodríguez-Rebolledo et al., 2015).

Incorporating soil–structure interaction into regional-scale subsidence predictions remains a significant challenge. Simplified empirical methods and design charts that modify the predicted greenfield displacements are among the most promising approaches to factor in the response of the foundations, e.g. the Modification Factor (MF) approach (Potts and Addenbrooke, 1997; Franzius et al., 2006). The MF approach, also known as the Relative Stiffness Method (RSM), has been extended to include the effects of pile foundations (Korff, 2013; Franza et al., 2017; Franza and Marshall, 2018). Currently, these methods only consider the immediate (or ultimate) deformations, e.g. from volume

* Corresponding author at: Department of Architecture and Civil Engineering, Chalmers University of Technology, Sweden.
*E-mail address:* pierre.wikby@chalmers.se (P. Wikby).

https://doi.org/10.1016/j.compgeo.2026.108410
Received 7 January 2026; Received in revised form 1 July 2026; Accepted 2 July 2026
Available online 17 July 2026

loss in excavations and tunnelling, and do not consider any change in the modification factors as a function of time. For floating pile foundations in deep deposits of soft clays, a time-independent modification factor might not be true, especially during the transient condition that starts with the (rapid) drawdown in the soil–rock interface. Therefore, for the large-scale modelling of subsidence due to underdrainage as a function of time, an alternative approach for the modification factors needs to be considered.

The neutral plane (NP) method is an elegant approach to predict the axial displacements at the head of a floating pile in a deep deposit of soft soils (Endo et al., 1969; Fellenius, 1971; Indraratna et al., 1992). NP is the plane of equal vertical displacements between the pile and the surrounding soil. This depth corresponds to where the sign of the (local) shaft friction changes from downdrag (negative) to resistance (positive). The location of NP can be estimated from the axial forces in the pile, assuming full mobilisation of the local shaft friction (Fellenius, 1971). Therefore, in compression, the NP becomes also the depth of maximum axial force in the pile and the depth of zero local shaft friction at the soil–pile interface. In reality, the location of NP depends on the interplay between the pile and the soil, and is therefore time-dependent (Indraratna et al., 1992; Wang and Brandenberg, 2013; Cao et al., 2014; Zhang et al., 2022; Liang et al., 2023; Ottolini et al., 2015). In most of the drawdown situations considered for the NP analysis, the largest settlements are towards the surface of the deposit (Auvinet and Hanell, 1981; Lee and Chen, 2003; Chen and Xiang, 2006), which is not the case in the underdrainage situations considered here (Rodríguez-Rebolledo et al., 2015). Similarly to the NP approach, the interaction level (IL) approach (Korff et al., 2016; Franza et al., 2021) estimates the plane of equal settlements. While the NP approach considers full mobilisation of the shaft resistance from the start of the calculation, the IL approach only considers additional settlements and shaft resistance developed from a reference point in time. This approach was therefore adopted here for estimating pile settlements caused by underdrainage.

This paper investigates the temporal evolution of interaction levels and modification factors for floating pile foundations subject to subsidence caused by underdrainage at the bottom of a soft clay deposit. After deriving the time-dependent modification factors from a systematic numerical study, the merits of the method are demonstrated for hypothetical scenarios of drawdown in central Gothenburg, Sweden.

## 2. Methodology

### 2.1. Finite element model

#### 2.1.1. Model geometry

A series of models were created with PLAXIS 2D v 2024.3 finite element (FE) software to study the response of a single pile subjected to underdrainage. The geometry and mesh are shown in Fig. 1. This is a reasonable approach for modelling settlement-driven development of negative skin friction, as the neutral plane of a single pile is nearly equal to or slightly shallower than that of a small pile group, see.e.g. Fellenius (2023). The axisymmetric model had a width of $100r_{pile}$, where $r_{pile}$ is the radius of the pile, to ensure that the pile response, and the drawdown are not affected by the right boundary. Consequently, a single pile is modelled, which is conservative in representing the main mechanism, i.e. the mobilisation of the neutral plane for floating pile rafts subjected to externally driven settlements (Lee and Chen, 2003). Furthermore, the width of the model ensures that the displacements obtained in $100r_{pile}$ are not affected by the pile, which simplifies the derivation of the modification factors. The layering consists of an aquifer system with a saturated low-permeable clay sandwiched in between an "upper" unconfined aquifer and a "lower" confined aquifer. The permeable clay fill (upper aquifer) and till (lower aquifer) layers have fixed thicknesses, while the thickness $H$ of the soft clay layer is varied in parametric analyses. The lower boundary of the numerical model is assumed to be fully-fixed, representing solid rock. Between 5795 and 6236 six-noded triangular elements (depending on $H$) were used. The size of the elements is approximately 3 cm in the material representing the pile and gradually increases towards the right-hand and lower model boundaries.

The pile length and pile radius of the reference problem were assumed to be $L_{pile} = 11$ m and $r_{pile} = 0.15$ m respectively, which is typical for old wooden piles. The tapering of the piles is not considered.

The lateral (left and right) and hydraulic boundaries were set to closed (no flow) as the boundary conditions for the pore pressures. Meanwhile, the longitudinal (top and bottom) were set to open (free flow), controlled by the assigned hydraulic heads.

#### 2.1.2. Constitutive models

The S-CLAY1S model (Karstunen et al., 2005) was adopted to model the natural soft clays that are representative of the study area, see Appendix A. The clayey fill was also modelled with S-CLAY1S, but with an increased vertical hydraulic conductivity, i.e. 0.1 m/day (ca. $10^{-6}$ m/s), emulating the effects of a fissured dry crust. The model parameters summarised in Tables 1 and 2 have been calibrated against site-specific data (see e.g. Haaf et al., 2024). The layer-dependent values were selected based on an overall interpretation of the site stratigraphy. While the measured permeability exhibits noticeable scatter, sensitivity analyses performed indicate that the variation has a negligible influence on the final results. Additionally, a validation of the undrained shear strength profile with test data near the site is provided in Appendix B.

The till layer and the pile were modelled using the Mohr–Coulomb and linear elastic models, respectively. The unit weight of the pile was set the same as that of the surrounding soil, in order to eliminate self-weight effects during the pile activation phase, and the stiffness of the pile is similar to that of a wooden pile. In the initial phase, the soft clay was modelled with a linear elastic model (Table 3) with a Poisson ratio of 0.38, corresponding to an earth pressure coefficient at rest of $K_0 = 0.6$, before initialisation of the state parameters of the S-CLAY1S model. The model parameters are shown in Table 3.

The pile interface was modelled with the Soft Soil model (Vermeer and Neher, 1999), with parameters equivalent to S-CLAY1S, see Table 2. Choosing the Soft Soil model reflects the fact that the clay surrounding the pile will be remoulded after pile installation (Isaksson and Dijkstra, 2025) thus affecting the interface. With the S-CLAY1S model as a user-defined model the properties of the interface would need to be fixed, which is not realistic, as both the strength and stiffness are stress-dependent. Same approach was employed in Tornborg et al. (2023) to smoothly model the changes in the interface stiffness between the clay represented by the Creep-SCLAY1S model and the foundation structure. The interface elements had a virtual thickness of 0.192 m and were assumed impermeable, as its permeability had negligible effect on resulting displacements. No reduction in strength or stiffness was prescribed. The interfaces were further considered to extend vertically downward and horizontally rightward from the corner of the pile toe, see Fig. 1. The interface extensions were applied to cope with the singularity in the corners due to the large stiffness gradient between the pile and the soil (Van Langen and Vermeer, 1991).

#### 2.1.3. Calculation phases

The calculation phases are summarised in Table 4 and further illustrated in Fig. 2. In the initial phase, hydrostatic conditions were assumed, with no additional loads present. The initial stress conditions in the model were created with gravity loading (Wikby et al., 2023). Subsequently, the elastic clay model was changed to the S-CLAY1S model. At this change, a new equilibrium is calculated without changing load or boundary conditions in a so-called plastic NIL step, and the state variables for S-CLAY1S were initialised, see e.g. Tornborg et al. (2021). Thereafter, the pile and its interface were activated, and the pile head load ($Q$) was applied, creating excess pore pressures and displacements in the clay. The pile installation effects were not

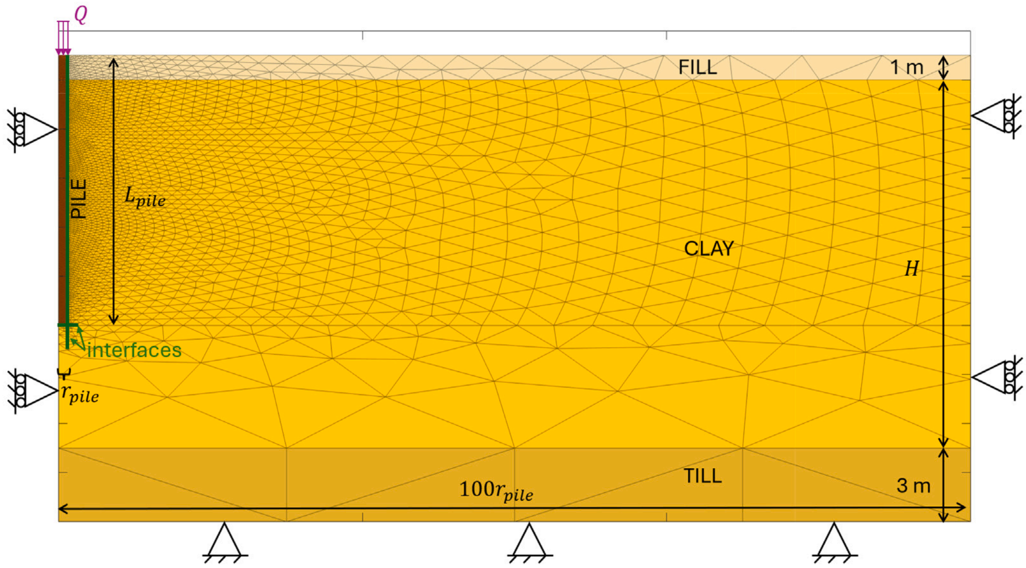


**Fig. 1.** The numerical model (not to scale) with mesh, boundary conditions, layers and materials: Example where $H$ = 15 m, $L_{pile}$ = 11 m and $r_{pile}$ = 0.15 m.

**Table 1**
Layer-dependent model parameters used for clay ad clay–pile interface.

| Layer | Unit weight $\gamma$ [kN/m$^3$] | Initial void ratio $e_0$ | Hydraulic conductivity $k$ [m/s] | Overconsolidation ratio ($OCR$) |
|---|---|---|---|---|
| Fill 0–1 m | 16 | 2.0 | $10^{-6}$ | 1.4 |
| Clay 1–11 m | 16 | 2.0 | $10^{-9}$ | 1.4 |
| Clay 11–21 m | 16 | 2.0 | $10^{-9}$ | 1.15 |
| Clay 21–24 m | 17 | 1.7 | $0.5 \times 10^{-9}$ | 1.1 |
| Clay 24–31 m | 17 | 1.7 | $0.5 \times 10^{-9}$ | 1.18 |
| Interface | 16 | 2.0 | Impermeable | 1.4 |

**Table 2**
Other model parameters used for clay and clay–pile interface.

| Material<br>Model<br>Parameter | Clay/Fill<br>S-CLAY1S<br>Value | Interface<br>Soft soil<br>Value |
|---|---|---|
| Coefficient of earth pressure at rest, $K_0$ | 0.6 | 0.6 |
| Poisson's ratio, $\nu'$ | 0.2 | 0.2 |
| Swelling index, $\kappa$ | 0.04 | 0.04[a] |
| Intrinsic compression index, $\lambda_i$ | 0.215 | – |
| Compression index, $\lambda$ | – | 0.215[a] |
| Stress ratio at critical state, $M$ | 1.45 | – |
| Cohesion, $c'$ [kPa] | – | 2 |
| Friction angle, $\phi'$ [°] | – | 35 |
| Initial anisotropy, $\alpha_0$ | 0.57 | – |
| Rate of rotational hardening, $\mu$ | 200 | – |
| Re. rate of rot. hardening due to dev. strain, $\beta$ | 1 | – |
| Initial amount of bonding, $x_0$ | 15 | – |
| Rate of destructuration, $a$ | 8 | – |
| Rate of destruct. due to deviatoric strain, $b$ | 0.5 | – |

[a] $\kappa = 0.013$ and $\lambda = 0.085$ was used for cases H30PWP10Q75 and H15PWP40Q75,100y to gain numerically stable results (see Table 5).

**Table 3**
Model parameters for till, pile and the clay layer during initial phase. MC = Mohr–Coulomb model, LE = Linear elastic model.

| Material | Till | Pile | Clay (initial) |
|---|---|---|---|
| Model | MC | LE | LE |
| Hydraulic conductivity, $k$ [m/s] | $10^{-6}$ | – | $10^{-9}$ |
| Unit weight, $\gamma$ [kN/m$^3$] | 18 | 16 | 16 |
| Poisson's ratio, $\nu$ | 0.2 | 0.3 | 0.38 |
| Elastic modulus, $E$ [MPa] | 30 | 5000 | 14 |
| Cohesion intercept, $c'$ [kPa] | 1 | – | – |
| Friction angle, $\phi'$ [°] | 35 | – | – |
| Dilation angle, $\psi$ [°] | 0 | – | – |

**Table 4**
Calculation phases used in the FE modelling.

| Phase | Description |
|---|---|
| Initialisation | Initial stress generation (gravity loading) + NIL step |
| Pile activation | Pile and interfaces activated |
| Pile head loading | Pile head loaded using $Q/Q_{ult}$ + consolidation |
| Drawdown | Drawdown + consolidation |

explicitly considered. The deviatoric strains, from loading the pile head, however, captured part of the change in the state of clay. The resulting excess pore pressures were allowed to fully dissipate (approximately 100–150 years) prior to the application of the drawdown scenarios.

In PLAXIS, an automated step size control (see e.g. Van Langen and Vermeer, 1990) is employed. The parameters controlling the load stepping, adopted the default values in PLAXIS with a global tolerance of 1%. A maximum of 10 time steps were stored to capture the load–displacement behaviour and the pore pressure development, respectively.

Firstly, a numerical pile load test (Fig. 3) was carried out in undrained conditions and an ultimate pile head load of $Q_{ult}$ = 199 kN was obtained from the load–displacement curve as annotated with a red arrow. Secondly, the normalised pile head load $Q/Q_{ult}$ was selected for each scenario in the parametric study.

The drawdown scenarios are based on potential leakage into a rock tunnel, which directly affects the magnitude of the pore pressures in the lower aquifer. The initial, transient, and final pore pressure profiles are visualised in Fig. 4(a). For the drawdown phase, the head in the lower aquifer is reduced, to model an instant pore pressure reduction due to the leakage. For the soft clay below the clayey fill, the final

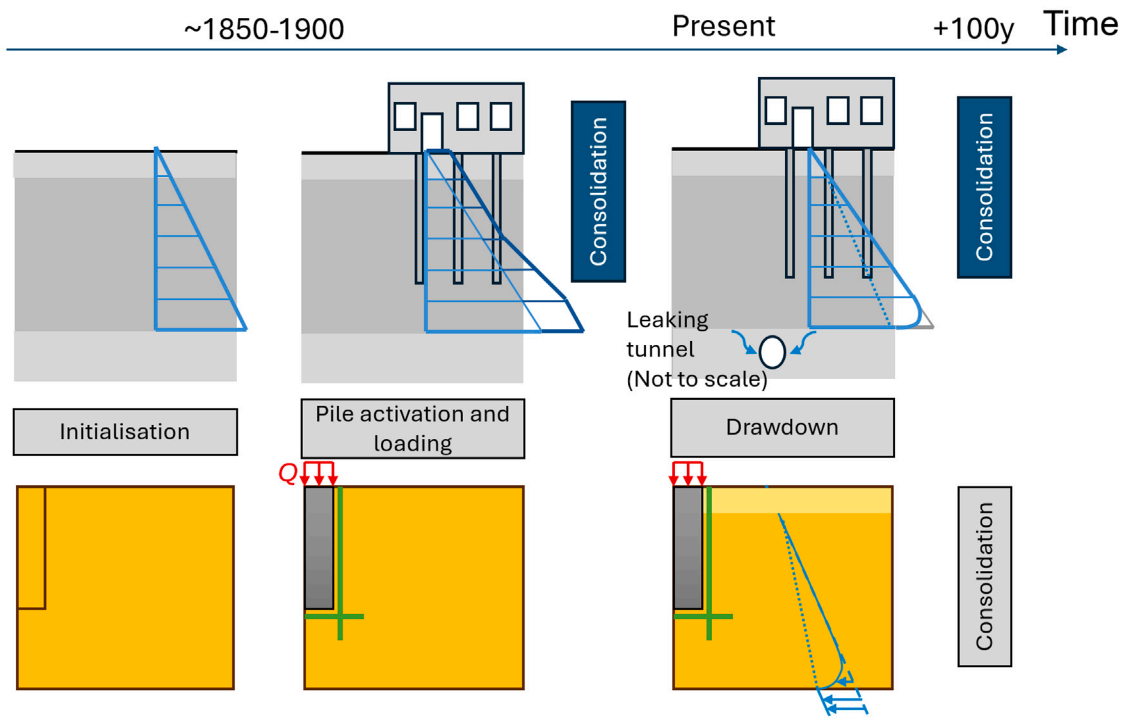


**Fig. 2.** Life cycle of a piled building undergoing subsidence due to a leaking tunnel. Idealisation (top) and the adopted numerical model (bottom).

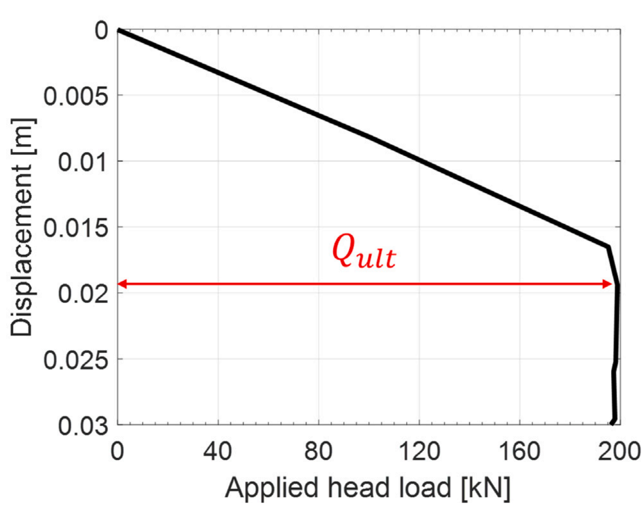


**Fig. 3.** Simulated pile load test.

pore pressures after full consolidation were interpolated between the pressure heads in the fill and till. Both the greenfield ($S^{gf}$) and pile ($S^{p}$) settlement profiles (Fig. 4b) were taken from cross-sections F-F′ and P-P′ in Fig. 4(a) for further analysis.

### 2.2. Parametric study

A parametric study was performed to investigate a range of hypothetical potential drawdown scenarios in the study area using the numerical modelling approach outlined above. The study area is located in central Gothenburg, where a new commuter train tunnel and station are being constructed. The construction of an unlined pre-grouted tunnel in hard crystalline rock will result in some leakage of groundwater into the tunnel, potentially reducing pore pressure levels in the soft clay above. The magnitude and duration of the leakage will impact the magnitude of the deformations in the soil, and hence the displacements at the pile head, over time. In the study area, there are deposits of soft sensitive marine clay that were formed during and after the last ice age (glacial and post-glacial clay). Below the soft clay layer, there are permeable layers of glacial till, occasional coarse-grained sediments (sand-gravel), and permeable fracture sets in weathered hard crystalline rock. Because of the latter, the extent of the leakage can be felt several hundreds of metres away from the actual construction, unless timely mitigation measures (e.g. additional sealing and infiltration) are implemented.

To cover a range of geometries for the pile foundation and soil depth, the parameters varied were; pore water pressure reduction (PWP), consolidation time after drawdown ($t$), clay thickness ($H$) and pile head load ($Q$). The PWP reductions were assumed to be 10 and 40 kPa, the same hypothetical scenarios used in Wikby et al. (2023), Haaf et al. (2024) and Wikby et al. (2024). For time-dependent scenarios, the responses in the short-term 3 months (annotated as 0.25y in the following) and 1 year (1y), as well as long-term 10 and 100-years (10y and 100y) conditions, were investigated. The short-term scenarios represent the time window in which mitigation measures are usually implemented if severe levels of subsidence are expected. The time factor $T_v$, further explained in Appendix C, was used as a normalisation parameter for the interaction levels and modification factors evaluated. Long-term scenarios include the designed life span of a tunnel with the modelled leakage. Three ratios for clay thickness over pile length $H/l$ (denoted H for the scenarios) were chosen to represent the large variation in clay thickness. Finally, the normalised pile head loads ($Q/Q_{ult}$) were chosen as 25%, 50% and 75% (denoted Q for the scenarios). A total of 18 scenarios (see Table 5) were analysed, considering the four consolidation times discussed above in each scenario.

### 2.3. Modification factor of settlements

The modification factor approach was developed by Potts and Addenbrooke (1997) to quantify the modification of the Gaussian greenfield settlement trough (deflection ratio and horizontal strains) from the effect of relative soil–structure stiffness in undrained tunnelling. The

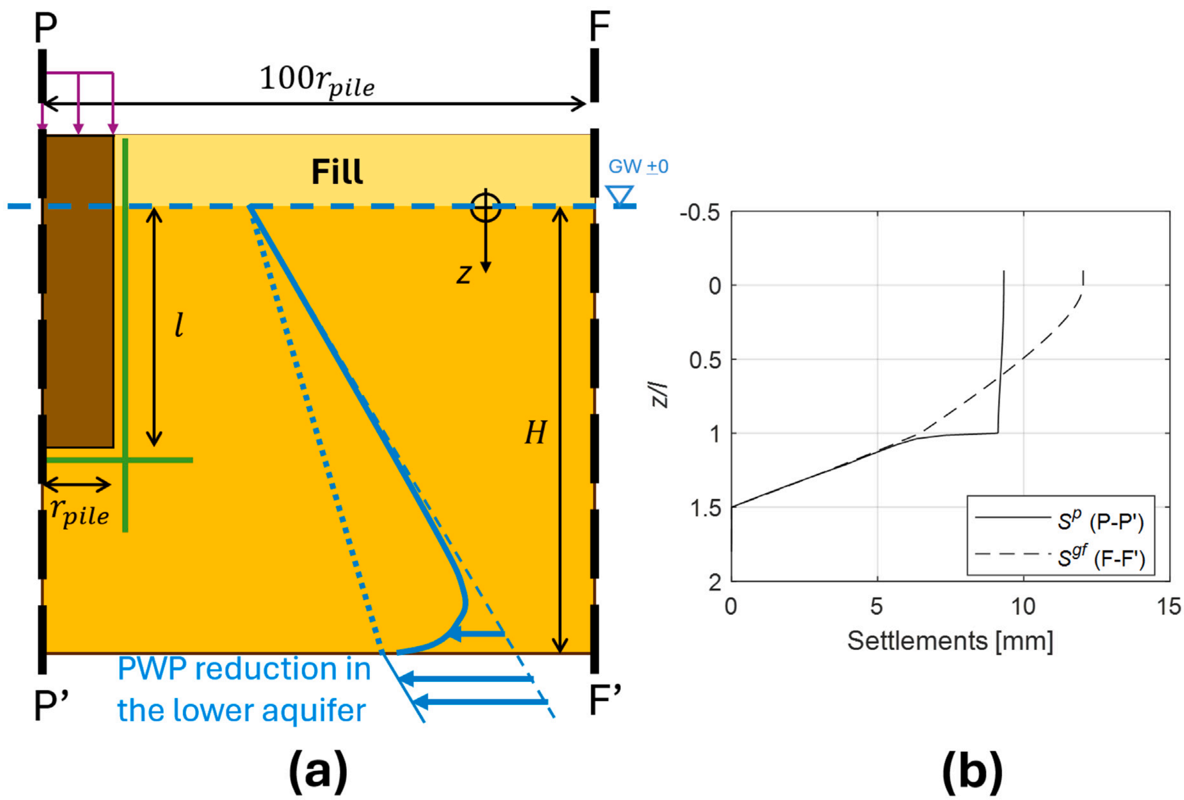


**Fig. 4.** (a) Modelling pore water pressure (PWP) reduction and consolidation. (b) Example of pile ($S^p$) and greenfield ($S^{gf}$) settlements from cross-sections P-P′ and F-F′.

**Table 5**
Scenarios modelled in the parametric study (time variation is left out).

| H/l, PWP | $Q/Q_{ult}$ = 25% | $Q/Q_{ult}$ = 50% | $Q/Q_{ult}$=75% |
|---|---|---|---|
| H/l = 1.5, PWP = 10 kPa | H15PWP10Q25 | H15PWP10Q50 | H15PWP10Q75 |
| H/l = 1.5, PWP = 40 kPa | H15PWP40Q25 | H15PWP40Q50 | H15PWP40Q75 |
| H/l = 2, PWP = 10 kPa | H20PWP10Q25 | H20PWP10Q50 | H20PWP10Q75 |
| H/l = 2, PWP = 40 kPa | H20PWP40Q25 | H20PWP40Q50 | H20PWP40Q75 |
| H/l = 3, PWP = 10 kPa | H30PWP10Q25 | H30PWP10Q50 | H30PWP10Q75 |
| H/l = 3, PWP = 40 kPa | H30PWP40Q25 | H30PWP40Q50 | H30PWP40Q75 |

approach has since been developed to account e.g. for building weight (Franzius et al., 2006; Giardina et al., 2015), facade openings (Giardina, 2013), and piled raft system (Franza and Marshall, 2018). Although the modification factor approach commonly considers the entire settlement trough of the foundation, since we deal with a purely axisymmetric single-pile problem, we quantify the modification due to the influence of piles in terms of subsidence rather than 2D settlement troughs. The modified subsidence ($MF^S$) thus becomes:

$$MF^S = S_0^p / S_0^{gf} \tag{1}$$

where $S_0^p$ and $S_0^{gf}$ are the numerically computed pile head and greenfield surface settlements, respectively.

Scenario-specific plots of $MF^S$ and $T_v$ (Fig. 5) were used to fit a trilinear function, with limiting values $T_1$, $T_2$, $MF_1$ and $MF_2$. The values $MF_1$ and $MF_2$ represent the values for short- and long-term modification factors respectively, while $T_1$ and $T_2$ represent the logarithmic values of time factors delimiting the short-, intermediate, and long-term values. The trilinear function is then integrated with a GIS database of the buildings, modelled as polygons in the study area, with attributes foundation type, construction year, average clay thickness, and greenfield settlements (computed as a function of pore pressure drawdown and time). The piled buildings constructed over 100 years ago were unlikely designed considering negative skin friction. However, the design of piled buildings younger than 100 years most likely had a safety factor applied. Hence, piled buildings older than 100 years were assumed to follow the load case of Q75 and the younger ones Q50, respectively. Once integrated with these classifications, the building-specific modification factors $MF^S$ were then combined with the results from a building damage model (Wikby et al., 2024), to assess the modification of the time-dependent building damage.

## 3. Individual pile response

Fig. 6 displays the greenfield and pile responses for scenario H15PWP40Q75. The changes in mean effective stress ($\Delta p'$), greenfield settlement ($S^{gf}$), normal effective stress at the pile–soil interface ($\sigma'_N$), shaft friction, and normalised axial pile load ($Q_z/Q_{ult}$) at four different consolidation times after drawdown (0y, 1y, 10y, and 100y) are plotted in Fig. 6. Note that the results are absolute, i.e. the effects of loads and displacement prior to the drawdown are included. The initial conditions (t = 0y) show that settlements, shaft friction and some axial load have developed as a result of the application of the pile head load. Over time, negative skin friction mobilises in the upper part of the pile, whereas positive shaft friction is mobilised fully after 100 years in the lower part of the pile.

The resulting greenfield settlement profiles as a function of depth for all scenarios are shown in Fig. 7. The results show as expected that settlement increase with larger pore pressure drawdown and thicker clay. The settlements are also further modified by the depth-dependent OCR profile (see Table 1), which is lower at depths $z/l > 1$, leading to a sharp increase in settlements in this region.

The results of pile settlements ($S^p$) in short- (3 months) and long-term (100 years) cases are plotted in Fig. 8. In general, a slight increase in $S^p$ is observed with increasing $Q$, while the majority of settlements occur beneath the pile toe, as a result of underdrainage and the lower

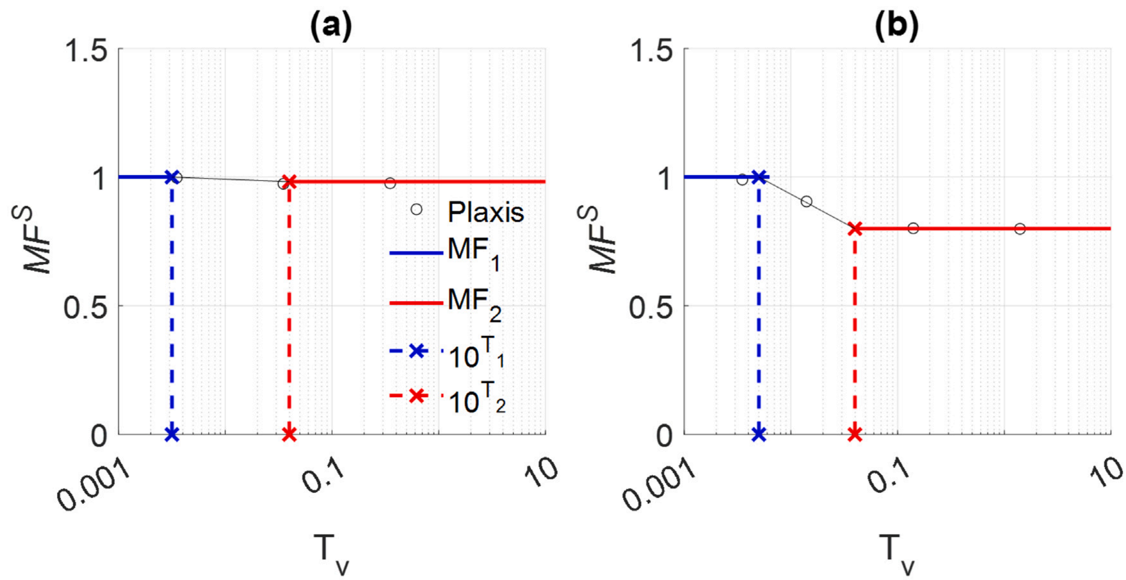


**Fig. 5.** Empirical lines created from the FE-resulted modification factors ($MF^S$) vs. time factor ($T_v$). Definition of variables $T_1$, $T_2$, $MF_1$ and $MF_2$ for the trilinear curve. Examples H15PWP40Q75 (a) and H15PWP10Q75 (b).

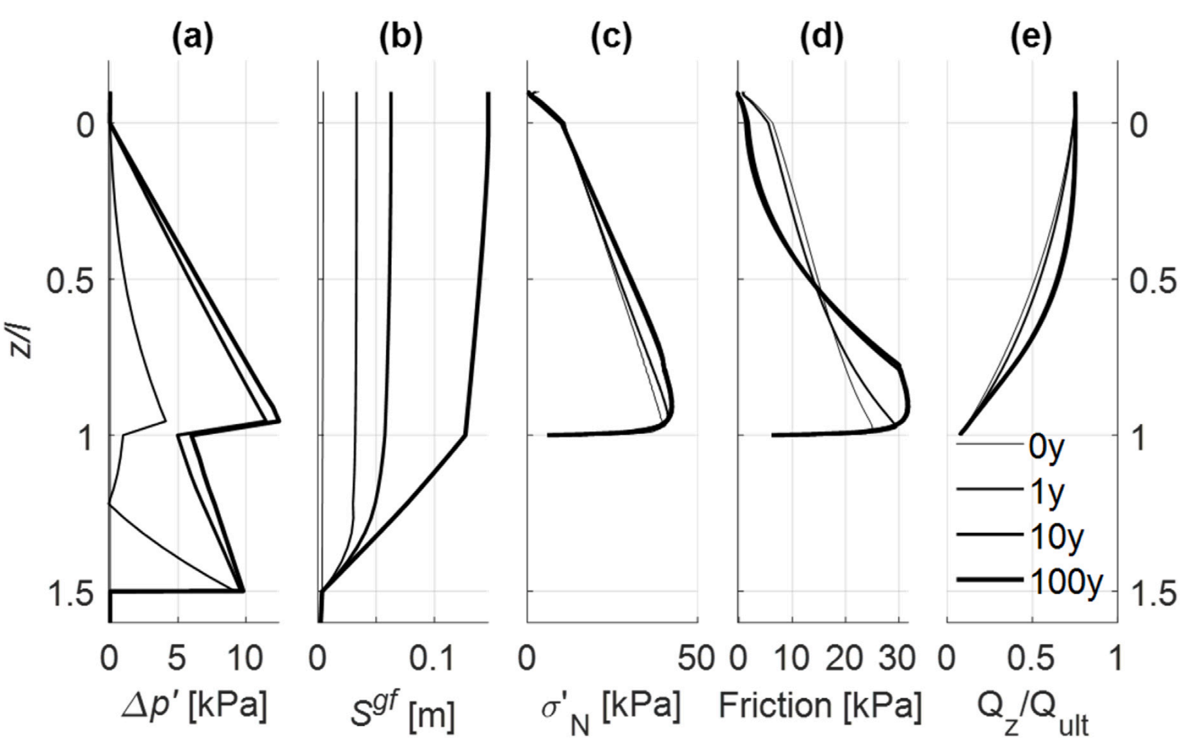


**Fig. 6.** Greenfield and pile response for the H15PWP40Q75 case at different consolidation times after drawdown: (a) Change in mean effective stress ($\Delta p'$). (b) Greenfield settlements ($S^{gf}$). (c) Normal effective stress ($\sigma'_N$). (d) Shaft friction. (e) Normalised axial pile load ($Q_z/Q_{ult}$).

OCR beneath the pile toe. Differences between the pile load cases are most evident for the scenario with the largest drawdown after 100 years of consolidation.

## 4. Generalised response

### 4.1. Interaction levels

The interaction levels ($z_i$), following the method of (Korff, 2013) as elaborated in Appendix D, were then calculated. Fig. 9 (left subplot) shows $z_i/l$ derived from pile and greenfield settlement profiles as a function of time for scenario H15PWP40Q75. Fig. 9 (right subplot) shows the predicted progression of $z_i/l$ as a function of the normalised time factor ($T_v$). In general, $z_i/l$ moves upward with increasing $T_v$.

Fig. 10 further shows the spread of $z_i/l$ when $Q$ is fixed for each individual plot. Generally, the upward trend with $T_v$ seen in Fig. 9 was found for all cases. Fig. 10 further shows that $z_i/l$ for some of the cases with large $Q$ are located at a shallower depth, while some exist in the deeper cluster, thus also displaying a larger variation in $z_i/l$. Similar results were found for the cases with larger PWP and smaller $H/l$.

Fig. 11 compares the numerically derived $z_i/l$ against simplified analytical approximations, such as $z_i/l$ at the 2/3-pile length and the

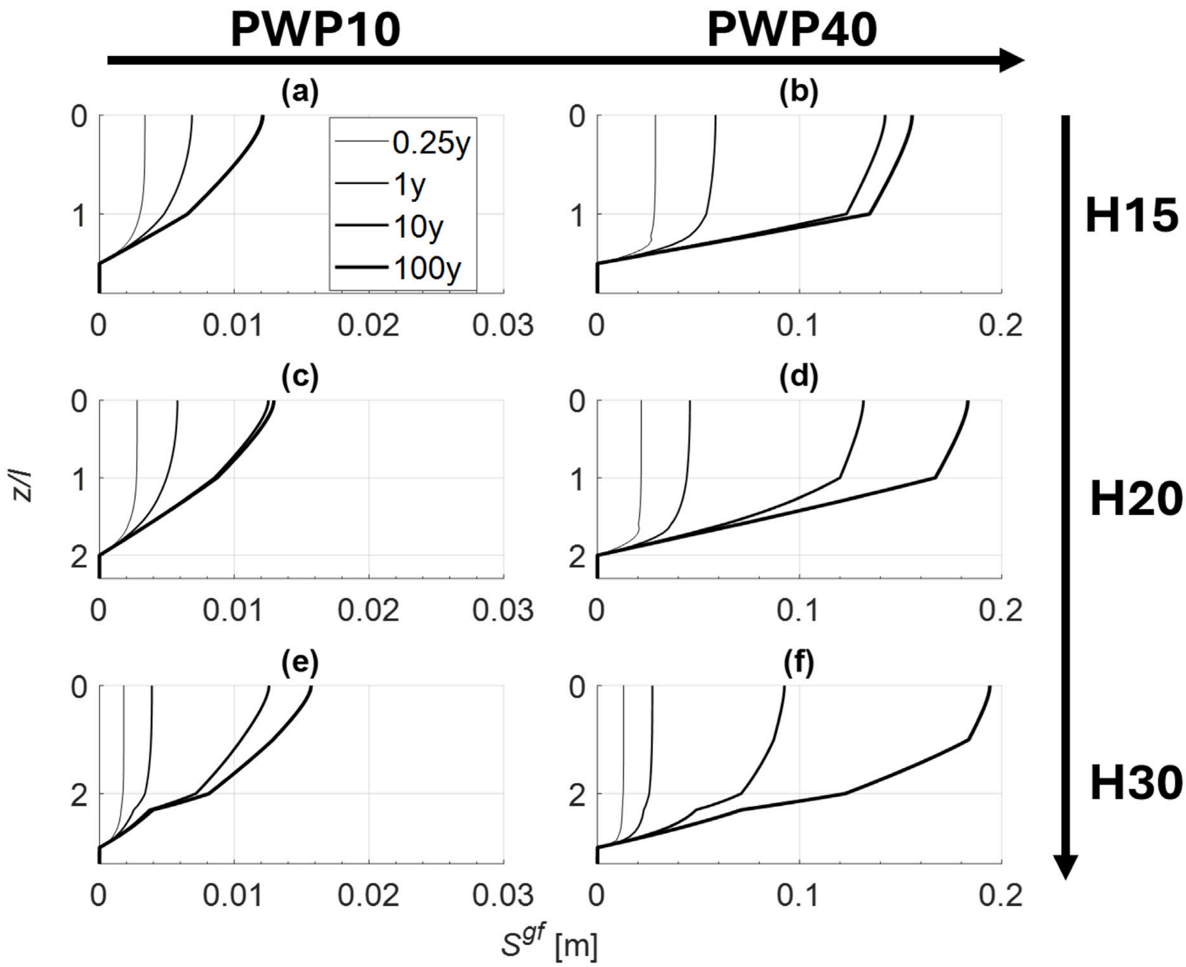


**Fig. 7.** Resulting greenfield settlement profiles for 3 months, 1 year, 10 years, and 100 years. PWP and H denote scenarios explained in Table 5.

$\alpha$-method; see Appendix D. A Consolidation Development Ratio ($CDR$) that quantifies a relative measure for the change in effective stress as function of the initial effective stress and the pre-overburden pressure (see Appendix C for definition) was introduced. $CDR$ characterises the effective stress conditions that impact the progression, shape, and magnitude of the greenfield settlement profiles. The figure shows that for the long-term cases, the simplified methods seem to work reasonably well, where the $\alpha$-method corresponds to the high-CDR cases (i.e. large PWP and small $H/l$) and the 2/3-line to the low-CDR cases. For short-term cases, the results are more scattered with values between 0 and 1, with the majority of the FE-based $z_i/l$ falling below the 2/3-line.

### 4.2. Modification factors

The data from the numerical analyses are subsequently used to derive the modification factors for the pile head displacements relative to the computed greenfield settlement. Fig. 12 shows the modification factor $MF^S$ for greenfield settlements as a function of normalised time $T_v$ after the start of the drawdown. The short-term ($T_v < 0.01$) modification factors remain 1, i.e. the resistance of the pile to subsidence is negligible ($MF^S = 1$). This is because most subsidence occurs initially below the pile base and the whole system settles. As consolidation gradually evolves towards the ground surface, some resistance of the pile develops, thus reducing the modification factor to a minimum of 0.8. The figure also highlights the results of the specific scenario of H15PWP40Q75, with a smaller reduction of $MF^S$ than in the other scenarios.

Fig. 13 shows the numerically-derived values of $MF^S$ (as open circles) separated in PWP- and load-specific scenarios as well as the fitted trilinear functions. For the PWP10 scenario, there is a clear long-term dependency of $MF^S$ on $H/l$. For example, H15 indicates a relatively small $MF^S$. The resistance of the pile to subsidence decreases with increasing $H/l$. Most settlements occur in the zone below the pile. In this scenario, the impact of the initial degree of mobilisation (effect of the pile head load) on $MF^S$ is negligible. A slight downward trend was assumed for both Q50 and Q75 in this drawdown scenario, to keep the functions simple and conservative.

## 5. Large-scale building damage model

### 5.1. Site description

The derived modification factors are used to assess the building damage for a hypothetical scenario for underdrainage in central Gothenburg, where many historic buildings are underpinned by floating wooden piles.

Fig. 14(a) shows a map of the buildings in the study area with their respective foundation types. The floating pile foundations (shown in dark grey) are further categorised by average clay thicknesses and construction year. These categories are presented as histograms showing the frequency of buildings in panels (b) and (c) of Fig. 14, respectively.

The older piled buildings (constructed before 1925) are expected to have nearly fully mobilised piles due to the limitations in pile design at the time. Therefore, the Q75 scenarios were assumed to be representative of older piled buildings, while the Q50 scenarios were assumed to represent the younger ones. These values are consistent with those assumed for old and young piled buildings in the

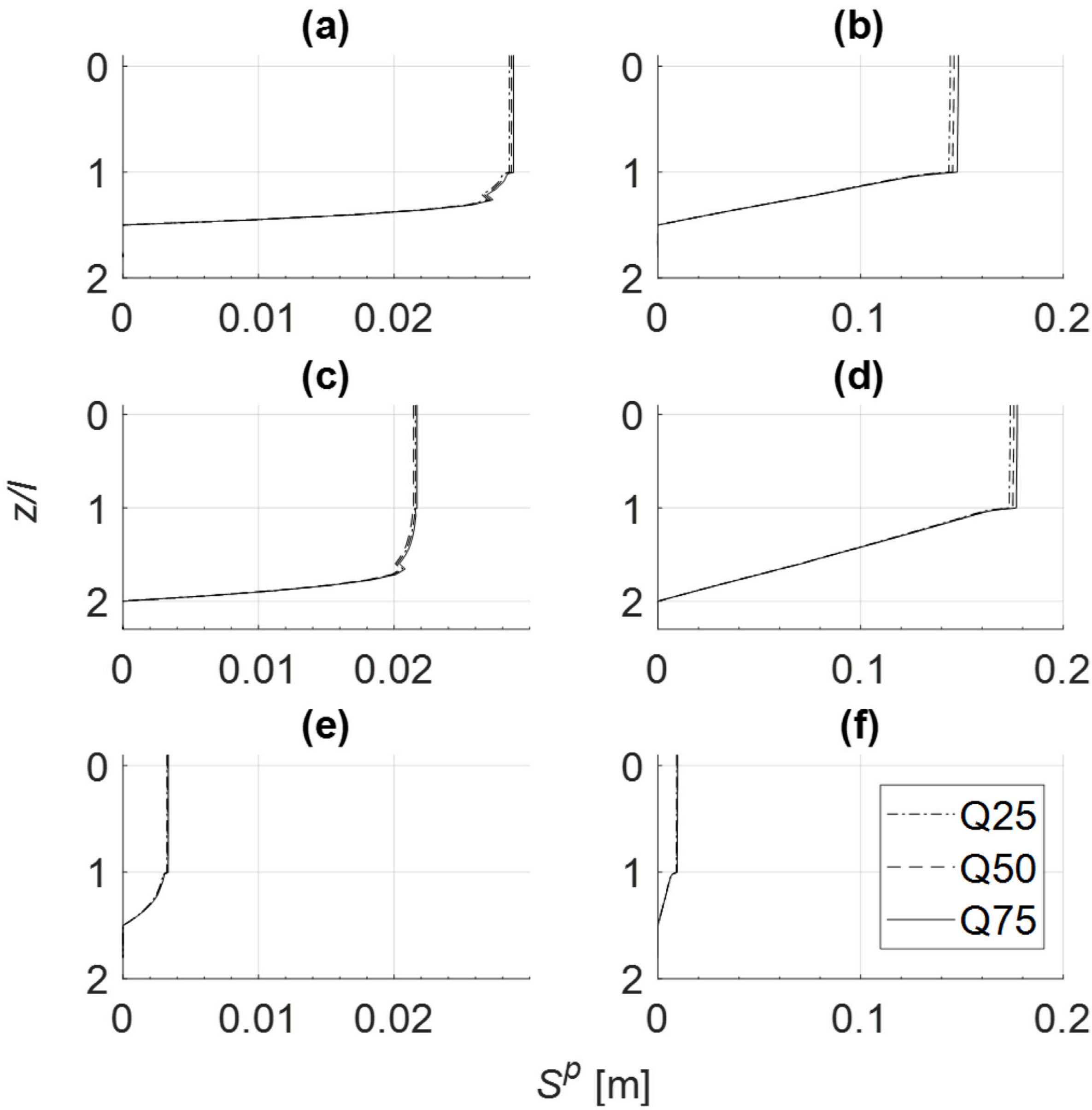


**Fig. 8.** Pile settlements ($S^p$) over normalised depth ($z/l$) for cases: H15PWP40 3 months (a) and 100 years (b). H20PWP40 3 months (c) and 100 years (d). H15PWP10 3 months (e) and 100 years (f).

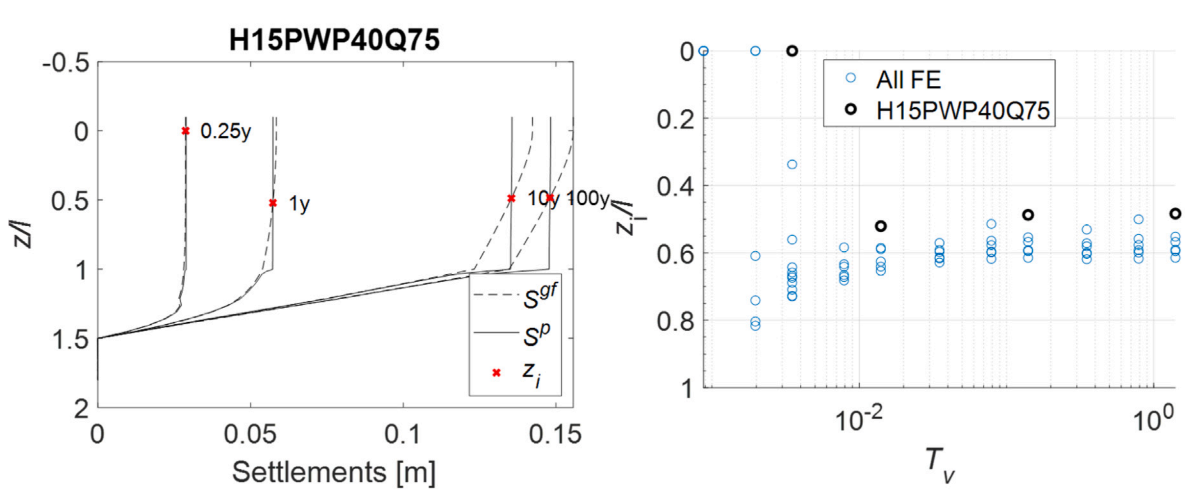


**Fig. 9.** Interaction levels ($z_i$) in relation to $S^{gf}$ and $S^p$ for example case H15PWP40Q75 (left). $z_i$ development over time factor ($T_v$) for all scenarios (right).

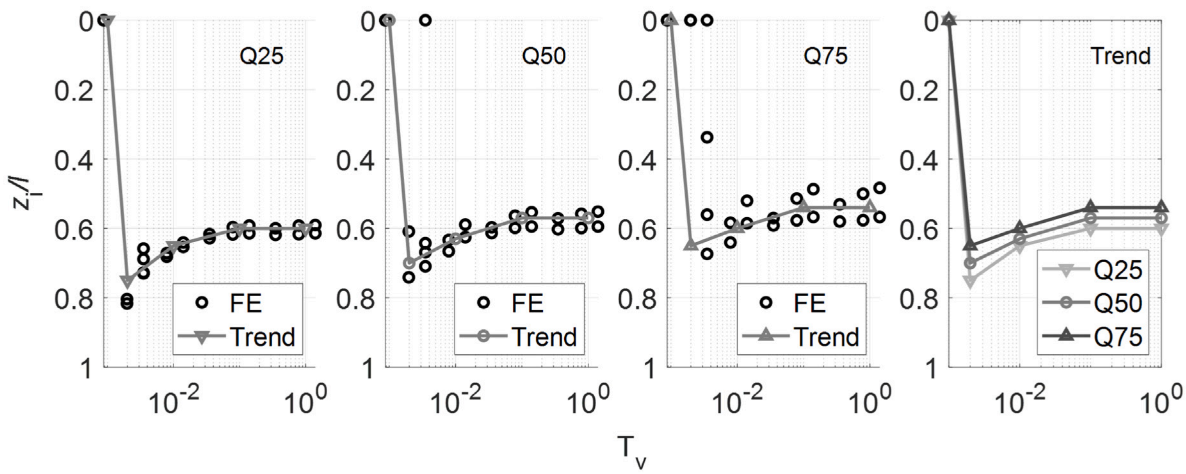


**Fig. 10.** Parametric influence of normalised load-specific scenarios (Q) on the interaction level. Plots of Q25, Q50 and Q75 (left). The trend of each plot (right). FE = Finite Element results.

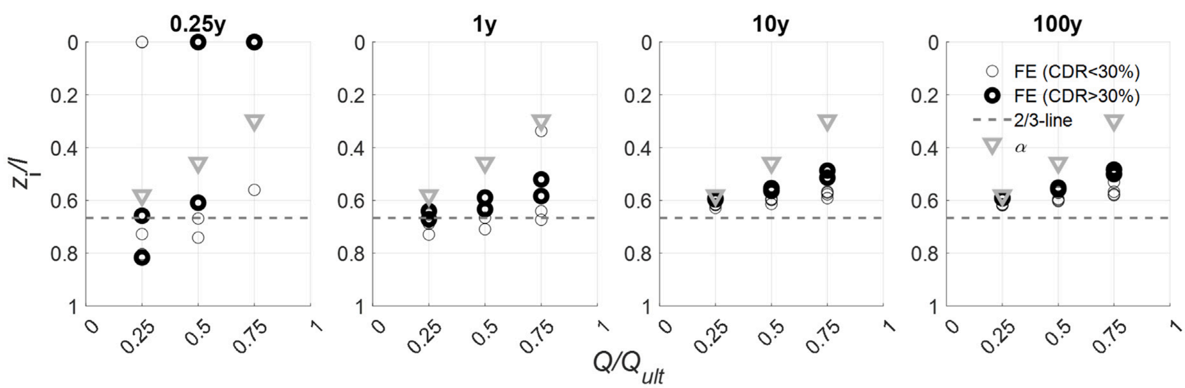


**Fig. 11.** Interaction level vs. pile head load case for all consolidation times. CDR values can be found in Appendix C. The results are compared with commonly used empirical methods ($\alpha$ and 2/3).

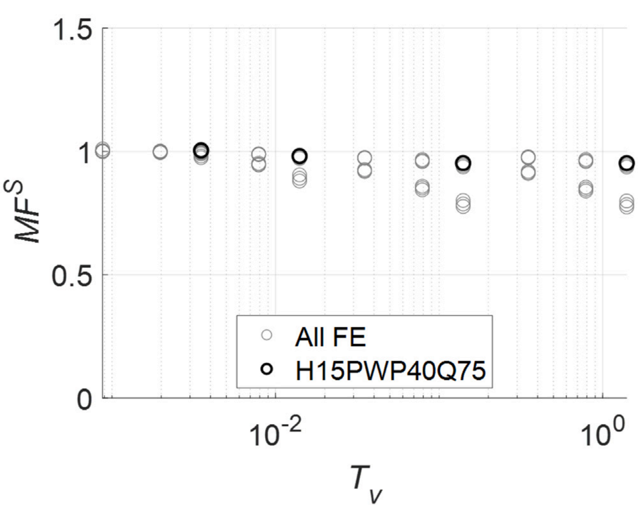


**Fig. 12.** Modification factor of settlements vs. time factor.

Netherlands (Korff et al., 2016). The trilinear curves derived in this work are used to calculate building-specific $MF^S$. For the results with 10 kPa pore pressure change, a maximum $MF^S = 1$ was used. The derived settlements incorporating these modification factors are then used together with the building damage model presented in Wikby et al. (2024) to calculate the updated damage classifications.

The damage criterion by Rankin (1988), with total settlement ($S$) and rotation ($\theta$) as parameters were adopted. The four damage classes are; negligible, slight, moderate, and high. For Rankin($S$) and Rankin($\theta$), these classes are defined by damage limits of 10, 50 and 75 cm, as well as 1/500, 1/200 and 1/50 respectively.

### 5.2. Impact on piled buildings

Fig. 15 shows the resulting $MF^S$ of buildings with floating pile foundations. Similarly, to Fig. 12, the 10 kPa results show the largest reduction in settlements. However, these vary with the clay thickness beneath each building. Moreover, a wider spread in settlement modification can be seen for buildings subjected to 10 kPa pore pressure drop compared to 40 kPa. As indicated by the histograms, the modification is around 10%–20% for 10 kPa and around 3% for 40 kPa.

Fig. 16 shows the predicted damage of buildings on floating piles when excluding the effect of piles (greenfield plots) and when including them (modified plots). The figure shows that damage is modified for more buildings using the Rankin($\theta$) criterion than the Rankin($S$) criterion, and that most of the assessments reduce from moderate to slight damage thanks to the presence of the piles.

Fig. 17 further shows that for the drawdown of 10 kPa, 1 building damage class was modified for the Rankin($S$) criterion, while 11 building damage classes (23%) were modified using the Rankin($\theta$) criterion. The most likely explanation for the higher sensitivity in the

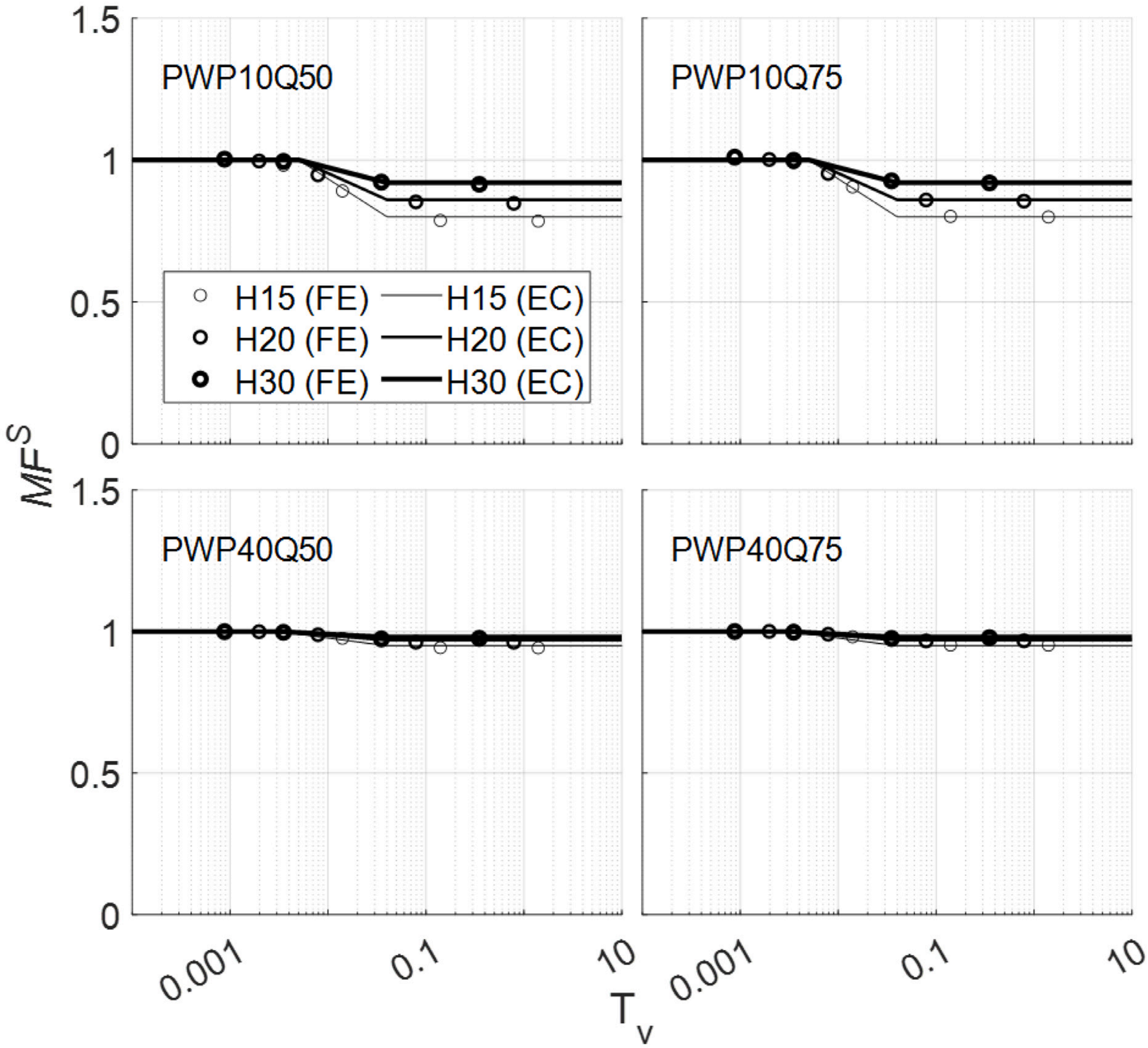


**Fig. 13.** Empirical functions (EC) created from the FE-resulted modification factors ($MF^S$) vs. $T_v$ for load scenarios Q50 and Q75. Hollow circles indicate FE results. Plots of load- and drawdown-specific cases of $MF^S$.

latter criterion is that lower levels of damage (slight to moderate) are predicted, which are defined by smaller intervals.

### 5.3. Discussion for case study

The case study demonstrates a simple, yet effective way of integrating the influence of piled buildings into large-scale assessments of building damage. Building damage is shown to decrease depending on the scenario and the criterion applied. A building predicted to be moderately damaged under greenfield conditions is more likely to be reduced to slight damage when the effects of the piles are incorporated, rather than from high to moderate damage.

Wikby et al. (2024) and Prosperi et al. (2023) recommended using 2D damage criteria based on differential settlements, such as rotation, as they are more related to the deformation of the superstructure than the total settlements. However, since only the 1D effects are covered here (vertical settlement modification due to a single pile), the 2D and 3D effects of the stiffness of the superstructure, the redistribution of loads on piles and pile group effects would eventually modify the settlement profile and thereby the predicted damage even further. It is therefore recommended that such effects are further investigated through more advanced modelling efforts. Due to their computational inefficiency, such numerical analyses should practically only be performed on buildings predicted with high-level damage using more simplified methods. This 2-stage approach was proposed by, e.g. Mair et al. (1996).

Alternatively, large-scale building damage could be predicted using settlement troughs calculated at the depth of the interaction level. Specifically, these depths could be approximated by the proposed interaction level charts or simplified methods (2/3 and $\alpha$), while settlement troughs could be derived from a physics-based metamodel (Haaf et al., 2024) trained on numerical results at such depths. Such an approach would generally be more consistent with the theory of interaction level than the modification factor approach adopted.

## 6. Conclusions

This paper proposes a numerical approach to study the impact of floating pile foundations on building damage in scenarios with pore pressure drawdown due to underdrainage. Time-dependent modification factors were derived from a systematic numerical study for several drawdown scenarios, pile head loads, and initial geometries using 2D Finite Element analyses. The derived modification factors were subsequently applied in large-scale predictions of damage due to subsidence for a Swedish case study.

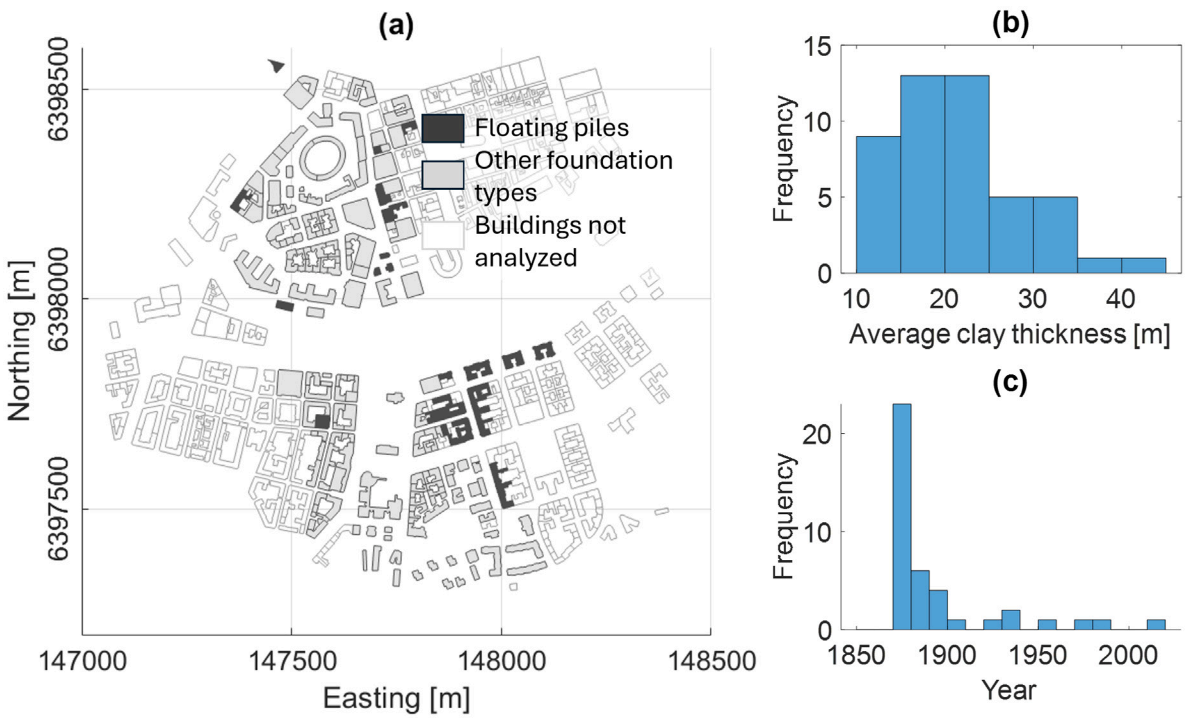


**Fig. 14.** Buildings in the study area with information on foundation type (a). Floating pile foundations with their frequency of (b) average clay thickness and (c) construction year.

The following conclusions can be drawn:

1. The modified settlements and hence interaction levels were shown to be time-dependent. Only long-term resistance to subsidence from the existence of floating piles was shown to be significant. This can be explained by the conditions of underdrainage, in which consolidation begins at the bottom of the deposit, thus producing insignificant initial settlements at the pile location.
2. There is a clear influence of the clay thickness and the magnitude of the drawdown on long-term modification factors, where the degree of mobilisation of the pile is most significant for extreme drawdown cases.
3. Long-term interaction levels can be approximated by simpler empirical methods, such as the $\alpha$-method for scenarios with high degree of mobilisation of the shaft resistance, and 2/3-pile level for smaller pile head loads.
4. The projected long-term damage was significantly reduced in the large-scale building damage predictions for buildings that had lower levels of damage under greenfield conditions.

## CRediT authorship contribution statement

**Pierre Wikby:** Writing – review & editing, Writing – original draft, Visualization, Validation, Software, Methodology, Investigation, Formal analysis, Conceptualization. **Ayman Abed:** Writing – review & editing, Visualization, Supervision, Software, Project administration, Methodology, Investigation, Conceptualization. **Minna Karstunen:** Writing – review & editing, Visualization, Supervision, Software, Resources, Project administration, Investigation, Funding acquisition. **Jelke Dijkstra:** Writing – review & editing, Visualization, Validation, Supervision, Methodology, Investigation, Formal analysis, Conceptualization.

## Declaration of competing interest

The authors declare that they have no known competing financial interests or personal relationships that could have appeared to influence the work reported in this paper.

## Acknowledgements

The research presented is financed by the Swedish Transport Administration (Trafikverket), grant number TRV 2020/54637. The work is done as part of the Digital Twin Cities Centre supported by Sweden's Innovation Agency VINNOVA under Grant No. 2024-03904.

## Appendix A. S-CLAY1S model in triaxial stress space

S-CLAY1S (Karstunen et al., 2005) is a critical-state model based on S-CLAY1 (Wheeler et al., 2003), to account for destructuration, in addition to plastic anisotropy. As it is mostly used for normal consolidated or lightly over-consolidated clays, isotropic elastic relationship is expressed in triaxial stress space as:

$$d\varepsilon_v^e = \frac{\kappa}{\upsilon p'} dp' \tag{A.1}$$

$$d\varepsilon_d^e = \frac{1}{3G} dq \tag{A.2}$$

where $\varepsilon_v^e$ and $\varepsilon_p^e$ represent for the elastic volumetric and elastic shear strain, respectively. $p'$ and $q$ denote the mean and deviatoric effective stresses, respectively, $\kappa$ is the swelling index, $\upsilon$ is the specific volume, and $G$ is the shear modulus. The yield surface is represented with an inclined ellipse, which can be expressed as:

$$F = (q - \alpha p') - (M^2 - \alpha^2)(p'_m - p')p' = 0 \tag{A.3}$$

where $M$ is the critical state stress ratio, $\alpha$ describes the inclination of the yield surface respective to the $p'$ axis, representing fabric anisotropy. $p'_m = (1 + x)p'_{mi}$ is the size of the yield surface, which is a function of intrinsic yield surface $p'_{mi}$ and any additional strength induced by bonding $x$.

The evolution of intrinsic yield surface follows the hardening rule in Cam-clay model:

$$dp'_{mi} = \frac{\upsilon p'_{mi}}{(\lambda_i - \kappa)} d\varepsilon_v^p \tag{A.4}$$

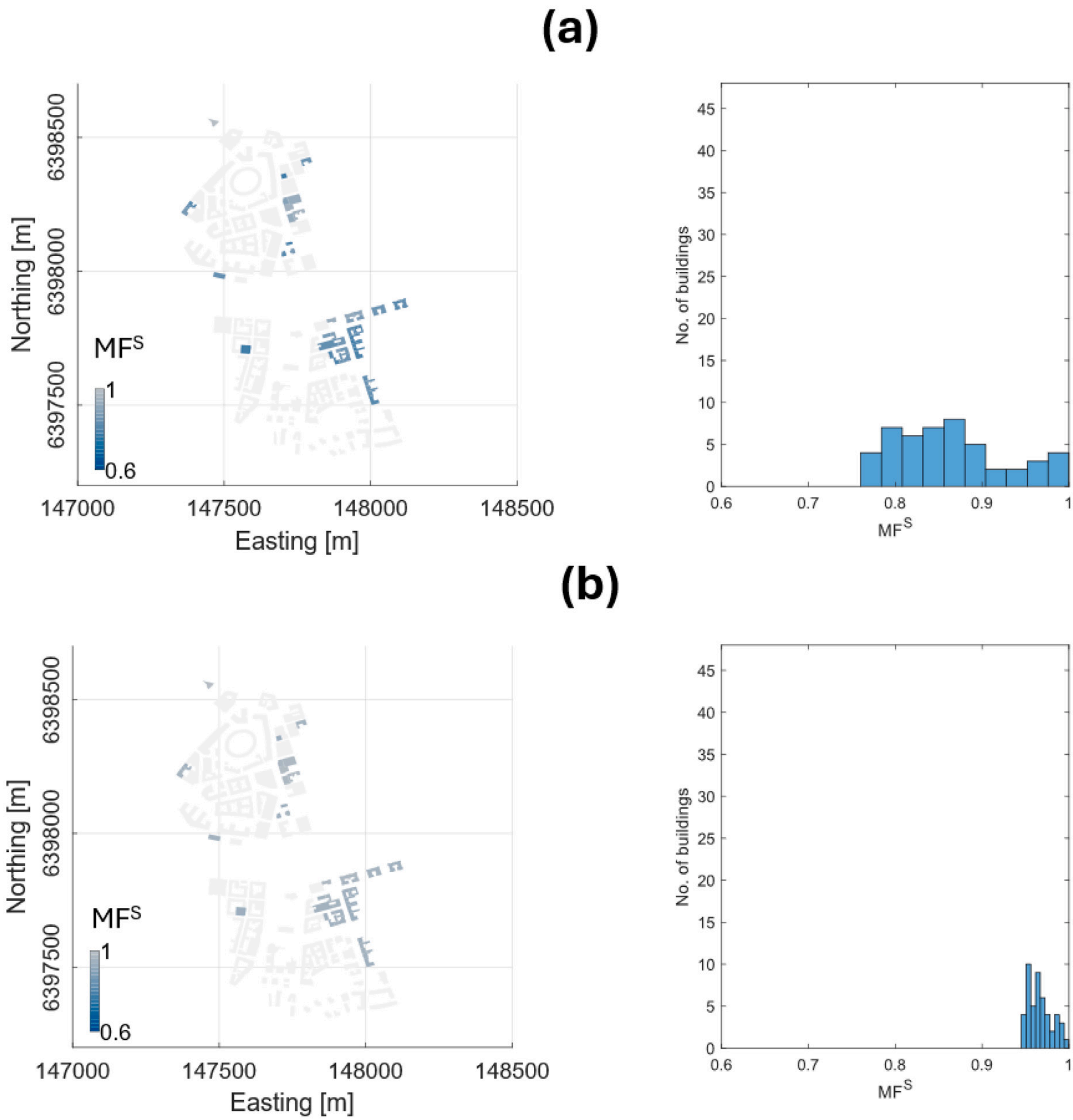


**Fig. 15.** Map of building-specific modification factor of settlements ($MF^S$) (left). Histograms for the computed building-specific $MF^S$ (right). Results after 30 years of (a) 10 kPa drawdown and (b) 40 kPa drawdown.

where $\lambda_i$ is the intrinsic compression index for natural clay, representing the steepest slope of the $\ln p' - \varepsilon_v$-curve from oedometer tests on reconstituted samples. $d\varepsilon_v^p$ is the plastic volumetric strain increment.

The destructuration is described by the evolution of $x$:

$$dx = -ax\left(\left|d\varepsilon_v^p\right| + bd\varepsilon_d^p\right) \tag{A.5}$$

where $a$ controls the rate of absolute destructuration, and $b$ denotes the relative effectiveness of plastic volumetric and plastic shear strain in destructuration.

In addition to isotropic hardening and destructuration, the evolution of fabric anisotropy is represented by the rotational hardening law:

$$d\alpha = \mu\left(\left[\frac{3p'}{4q} - \alpha\right]\langle d\varepsilon_v^p\rangle + \beta\left[\frac{p'}{3q} - \alpha\right]\left|d\varepsilon_d^p\right|\right) \tag{A.6}$$

where $\langle\rangle$ are Macaulay brackets, ensuring that the model predictions remain sensible when $d\varepsilon_v^p < 0$, $\mu$ governs the absolute rate of the rotation of the yield surface and $\beta$ describes the relative effectiveness of volumetric and plastic shear strains in rotation.

In order to initialise the state parameters of S-CLAY1S, i.e., fabric anisotropy $\alpha$ and bonding amount $x$, a $K_0$ loading history is assumed. Thus, the initial anisotropy, $\alpha_0$, can be estimated as a function of the normally consolidated coefficient of earth pressure at rest $K_{0(NC)}$ loading:

$$\eta_{K_0} = \frac{3(1 - K_{0(NC)})}{1 + 2K_{0(NC)}} \tag{A.7}$$

$$\alpha_0 = \frac{\eta_{K_0}^2 + 3\eta_{K_0} - M^2}{3} \tag{A.8}$$

According to Jaky's formula, $K_{0(NC)} = 1 - \sin\phi'$, where $\phi'$ is the friction angle.

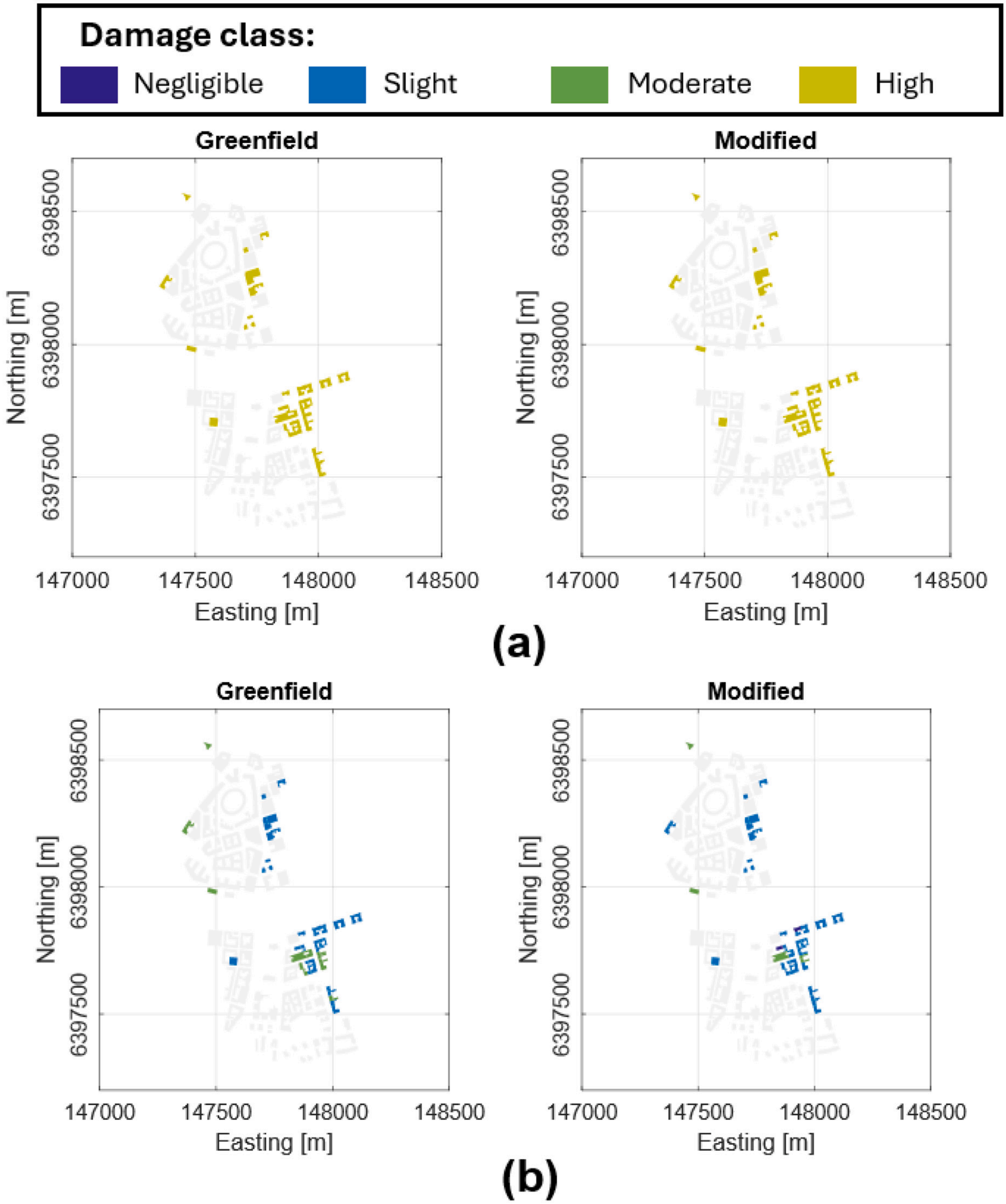


**Fig. 16.** Map of building damage after 30 years of 10 kPa drawdown without the effect of piles (left) and with piles (right). Damage classification according to Rankin (1988) using damage parameters (a) Total settlements ($S$) and (b) Rotation ($\theta$).

The initial value $x_0$ representing the amount of bonding is linked to the sensitivity $S_t$:

$$x_0 = S_t - 1 \tag{A.9}$$

where $S_t$ is derived from the fall cone tests in laboratory as the ratio of the shear strengths of an intact and a remoulded sample.

## Appendix B. Validation of undrained shear strength

The undrained shear strength profile predicted by the model was validated against laboratory test data on nearby samples from Tornborg et al. (2024), see Fig. B.1. The numerical tests were performed in PLAXIS soil test in undrained conditions using the same input values of S-CLAY1S as for the subsequent numerical analyses, see Table 2.

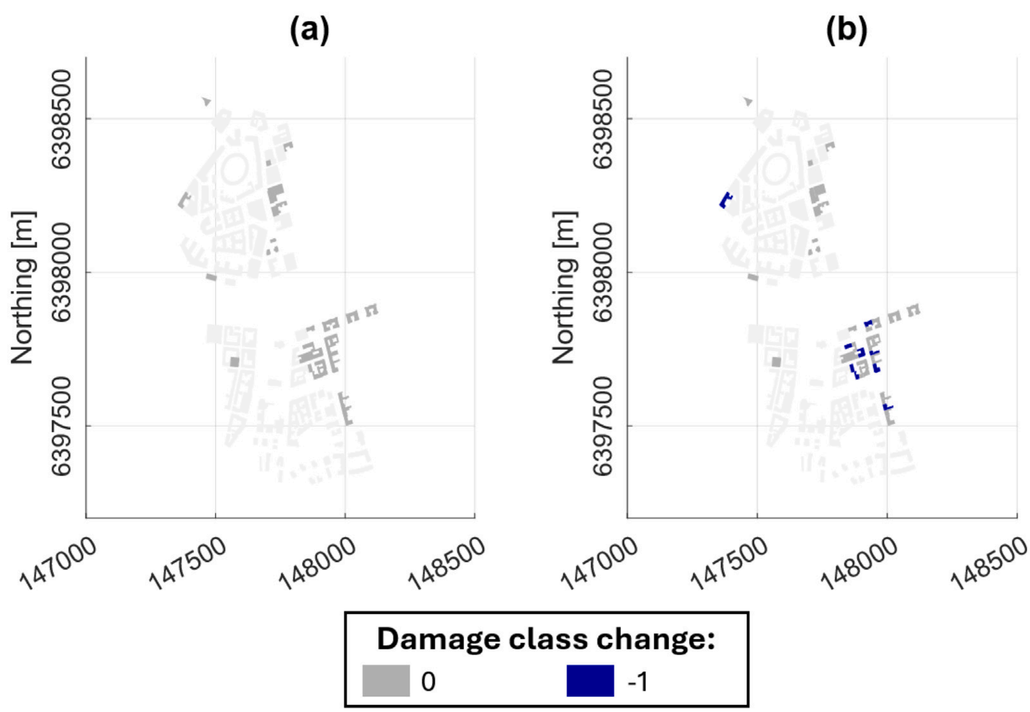


**Fig. 17.** Change in damage class for 30 years, 10 kPa drawdown. Blue buildings represent a reduction of one damage class using (a) Rankin (1988) ($S$) and (b) Rankin (1988) ($\theta$).

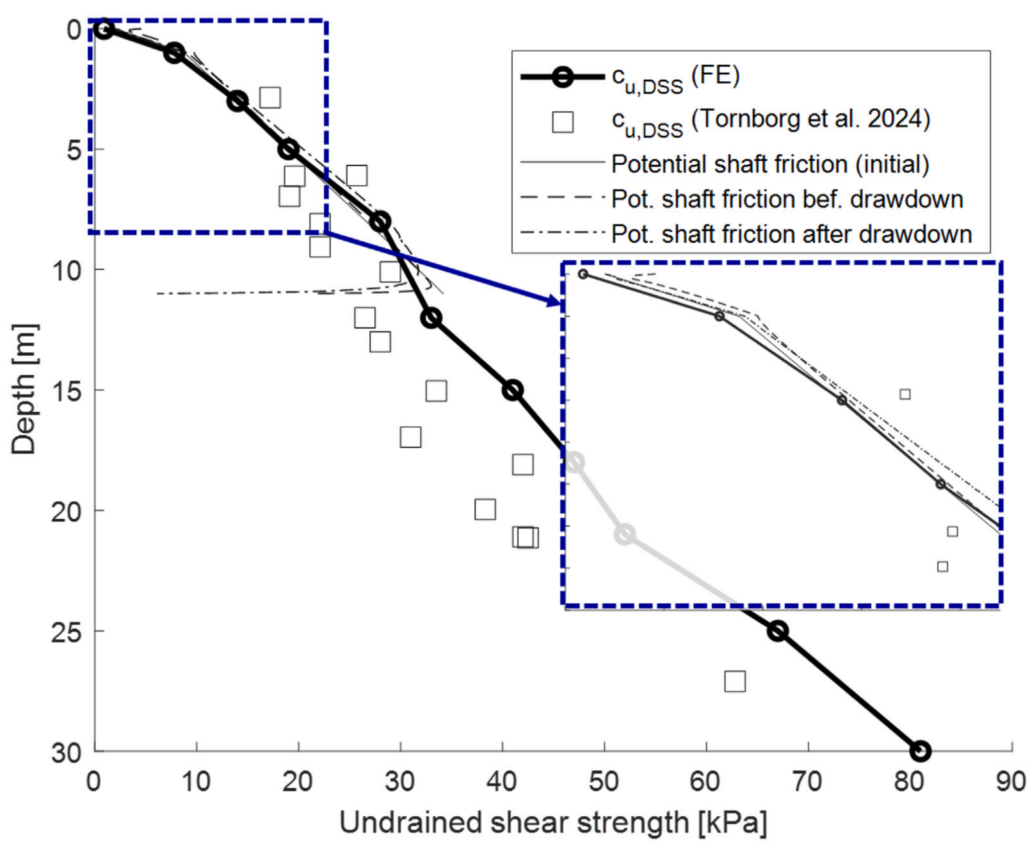


**Fig. B.1.** Numerical vs. laboratory results of undrained shear strength from direct simple shear (DSS) tests, $c_{u,DSS}$, in Gothenburg (Tornborg et al., 2024). Additionally, the profile of the potential shaft friction over time was added to inform the selection of the adhesion factor, $\alpha$.

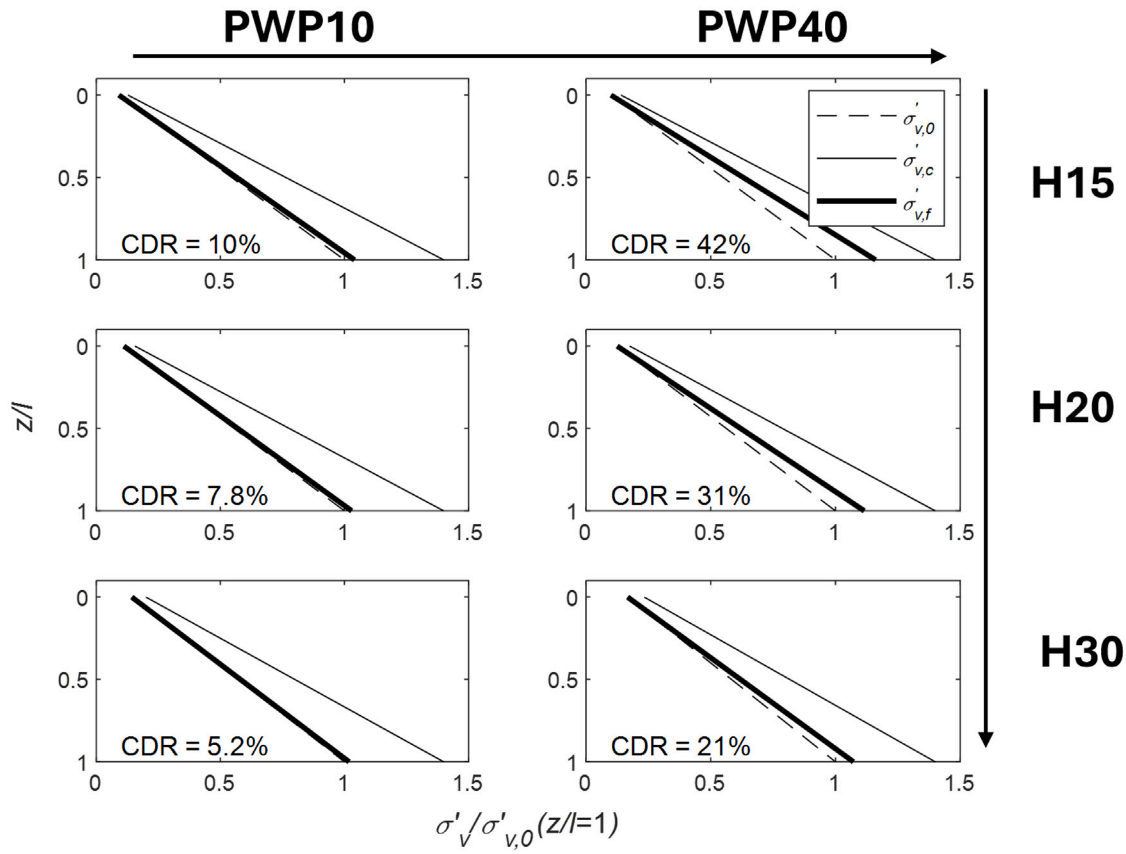


**Fig. C.1.** Effective (vertical) stress ($\sigma'_v$) normalised to effective initial stress at pile toe level ($\sigma'_{v,0}(z/l = 1)$) profiles and CDR values for the different scenarios. $\sigma'_{v,0}$ = initial effective stress, $\sigma'_{v,c0}$ = apparent preconsolidation pressure, $\sigma'_{v,f}$ = final effective stress.

## Appendix C. Definition of consolidation parameters

### C.1. CDR

To study the degree of mobilisation of skin friction, the vertical effective stresses before the reduction of pore pressure ($\sigma'_{v,0}$) and after full consolidation ($\sigma'_{v,f}$) were compared with the apparent vertical preconsolidation pressure prior to pile installation ($\sigma'_{v,c0}$) as a function of depth see Fig. C.1. The values at the bottom for each profile were then used to calculate Consolidation Development Ratio at full consolidation ($CDR$) as:

$$CDR = (\sigma'_{v,f} - \sigma'_{v,0})/(\sigma'_{v,c0} - \sigma'_{v,0}) \tag{C.1}$$

At $CDR = 0$, there is no increase in effective stress and thus no settlements. $CDR \geq 1$ equals to the complete development of elastoplastic strains, while values ranging between 0 and 1 contain the onset of yield, due to the formulation of the S-CLAY1S model that allows for strain softening.

### C.2. Time factor

To study the time dependence of the interaction levels and modification factors, they were normalised according to the time factor:

$$T_v = (c_v t)/H^2 \tag{C.2}$$

where a constant coefficient of consolidation $c_v = 10^{-7}$ m$^2$/s was chosen.

## Appendix D. Analysis of interaction level

### D.1. Interaction levels from FE

Time-dependent interaction levels ($z_i$) were derived to see at what depth the pile and greenfield settlements are equal. Here, $z_i$ for time $T$ is defined as the point of equal greenfield $S^{gf}$ and pile settlements $S^p$ after the initial settlements (unrelated to the drawdown, $t = 0$) have been reduced.

$$S^p(z_i, t = T) - S^p(z_i, t = 0) = S^{gf}(z_i, t = T) - S^{gf}(z_i, t = 0) \tag{D.1}$$

According to theory, $z_i$ would be equal to the neutral plane (NP) only if the full friction is mobilised throughout the entire length of the pile. However, for long transition zones, i.e. where skin friction is not yet fully mobilised, $z_i$ is significantly different from the actual NP (Korff et al., 2016). $z_i$ could also be used along with depth-dependent greenfield profiles from large-scale settlement models (Haaf et al., 2024) to predict damage to piled buildings.

According to Korff et al. (2016) and Franza et al. (2021), $z_i$ is a function of:

- the normalised pile head load - $Q/Q_{ult}$,
- the normalised base resistance - $Q_b/Q_{ult}$, where $Q_b$ is the base resistance of the pile,
- the normalised gradient of soil settlement - $(S_0^{gf} - S_l^{gf})/S_{ult}$, where $S_0^{gf}$ and $S_l^{gf}$ are the greenfield settlements on the surface and at the level of pile toe, respectively, and $S_{ult}$ is the relative displacement between the pile and soil at ultimate bearing capacity,

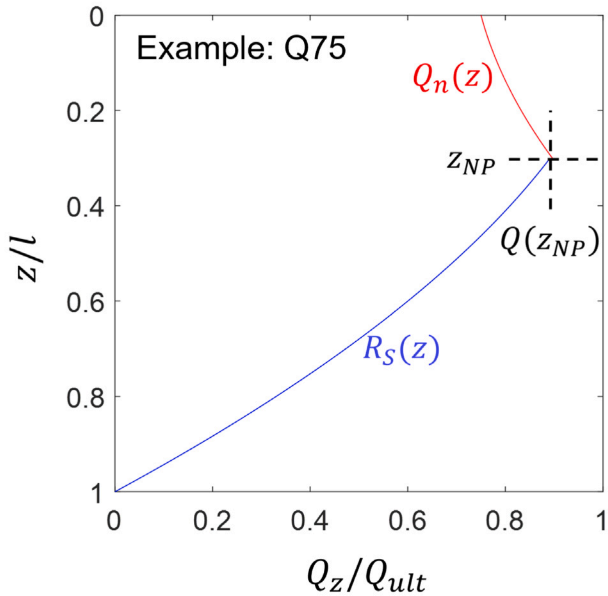


**Fig. D.1.** Axial load distribution for a fully mobilised pile with normalised load Q75 according to the empirical solution using the $\alpha$-method. $R_s$ is the shaft resistance, $Q_n$ is the dragload, and $z_{NP}$ is the neutral plane depth.

- the ultimate skin friction gradient ($\tau_{max,l}/\tau_{max,0}$), where $\tau_{max,l}$ and $\tau_{max,0}$ are the ultimate skin frictions at the pile toe and ground level, respectively, as well as
- the normalised pile diameter ($D/S_{ult}$).

In our case, $Q_b/Q_{ult}$ is negligible for floating piles, $D/S_{ult}$ and $\tau_{max,l}/\tau_{max,0}$ is roughly the same for all scenarios.

### D.2. Neutral plane from empirical approaches

The locations of the interaction level derived numerically were compared to empirically calculated neutral planes ($\alpha$, 2/3) to see whether simplified methods could be used.

In the total stress-based $\alpha$-approach (Tomlinson, 1957), the shaft friction is assumed to be fully mobilised over the entire pile length for each load-specific case (Q25, Q50 and Q75). Meanwhile, the base resistance is neglected for long slender floating piles in clay typically used in Sweden (also the base resistance is similar to the self-weight of the pile). For ultimate shaft friction, the dragload (or negative skin friction, $Q_n$) and resistance (or positive skin friction, $R_s$) were first calculated for a cylindrical pile with constant radius ($r_{pile}$ [m]):

$$Q_n(z) = \int_0^z 2\pi r_{pile}\tau_s(z)dz \tag{D.2}$$

$$R_s(z) = \int_z^{L_p} 2\pi r_{pile}\tau_s(z)dz \tag{D.3}$$

where $\tau_s$ [kPa] is the unit shaft friction:

$$\tau_s(z) = \alpha c_u(z) \tag{D.4}$$

The $\alpha$-method is commonly used for floating piles in the soft soils of Sweden. $\alpha = 1$, inferred from Fig. B.1, was chosen. The undrained shear strength ($c_u(z)$) for the current work was retrieved by simulation results presented in Fig. B.1. Once $Q_n$ and $R_s$ were calculated along the pile shaft, $z_{NP}$ was finally calculated:

$$Q + Q_n(z_{NP}) = R_s(z_{NP}) \tag{D.5}$$

An example of how $z_{NP}$ was derived for the Q75 scenario is shown in Fig. D.1. In addition to the neutral planes derived by the $\alpha$-method, the commonly assumed neutral plane at a depth of 2/3 of the pile length is also compared with the interaction levels derived by numerical analyses.

## Data availability

Data will be made available on request.

## References

Auvinet, G., Hanell, J., 1981. Negative skin friction on piles in Mexico City clay. In: Proceedings Ofthe 10th International Conference on Soil Mechanics and Foundation Engineering. Vol. 2, A. A. Balkema, Stockholm, pp. 559–604.

Cao, W., Chen, Y., Wolfe, W.E., 2014. New load transfer hyperbolic model for pile-soil interface and negative skin friction on single piles embedded in soft soils. Int. J. Geomech. 14 (1), 92–100. http://dx.doi.org/10.1061/(asce)gm.1943-5622.0000289.

Chen, S., Xiang, Y., 2006. A procedure for theoretical estimation of dewatering-induced pile settlement. Comput. Geotech. 33 (4–5), 278–282. http://dx.doi.org/10.1016/j.compgeo.2006.05.002.

Endo, M., Minou, A., Kawasaki, T., Shibata, T., 1969. Negative skin friction acting on steel pipe pile in clay. In: Proceedings of the 7th International Conference on Soil Mechanics and Foundation Engineering. Mexico City, pp. 85–92. http://dx.doi.org/10.1016/0266-1144(84)90012-8.

Fellenius, B.H., 1971. Negative Skin Friction on Long Piles Driven in Clay. Tech. Rep., Swedish Geotechnical Institute (Proceedings No. 25), Stockholm, pp. 901–921.

Fellenius, B.H., 2023. Basics of Foundation Design (Electronic). pp. 1–546.

Franza, A., Marshall, A.M., 2018. Centrifuge modeling study of the response of piled structures to tunneling. J. Geotech. Geoenvironmental Eng. 144 (2), 04017109. http://dx.doi.org/10.1061/(asce)gt.1943-5606.0001751.

Franza, A., Marshall, A.M., Haji, T., Abdelatif, A.O., Carbonari, S., Morici, M., 2017. A simplified elastic analysis of tunnel-piled structure interaction. Tunn. Undergr. Space Technol. 61, 104–121. http://dx.doi.org/10.1016/j.tust.2016.09.008.

Franza, A., Marshall, A.M., Jimenez, R., 2021. Non-linear soil–pile interaction induced by ground settlements: Pile displacements and internal forces. Geotechnique 71 (3), 239–249. http://dx.doi.org/10.1680/jgeot.19.P.078.

Franzius, J.N., Potts, D.M., Burland, J.B., 2006. The response of surface structures to tunnel construction. Proc. Inst. Civ. Eng. - Geotech. Eng. 159 (1), 3–17. http://dx.doi.org/10.1680/geng.2006.159.1.3.

Giardina, G., 2013. Modelling of Settlement Induced Building Damage (Doctoral dissertation). TU Delft, p. 291.

Giardina, G., DeJong, M.J., Mair, R.J., 2015. Interaction between surface structures and tunnelling in sand: Centrifuge and computational modelling. Tunn. Undergr. Space Technol. 50, 465–478. http://dx.doi.org/10.1016/j.tust.2015.07.016.

Haaf, E., Wikby, P., Abed, A., Sundell, J., McGivney, E., Rosén, L., Karstunen, M., 2024. A metamodel for estimating time-dependent groundwater-induced subsidence at large scales. Eng. Geol. 341 (August), http://dx.doi.org/10.1016/j.enggeo.2024.107705.

Hoffmann, J., Leake, S., Galloway, D., Wilson, A.M., 2003. MODFLOW-2000 Ground-Water Model—User Guide to the Subsidence and Aquifer-System Compaction (SUB) Package. Tech. Rep., US Geological Survey, Tucson, AZ, p. 46, US Geological Survey Open-File Report 03-233.

Indraratna, B., Balasubramaniam, A.S., Phamvan, P., Wong, Y.K., 1992. Development of negative skin friction on driven piles in soft Bangkok clay. Can. Geotech. J. 29 (3), 393–404. http://dx.doi.org/10.1139/t92-044.

Isaksson, J., Dijkstra, J., 2025. Modeling the pile cycle of an axially loaded pile in sensitive natural clay. J. Geotech. Geoenvironmental Eng. 151 (7), 1–15. http://dx.doi.org/10.1061/jggefk.gteng-13179.

Karlsrud, K., Sander, L., 1978. Subsidence problems caused by rock-tunnelling in Oslo. In: International Conference on Evaluation and Prediction of Subsidence. Pensacola Beach, Fla, pp. 1–10.

Karstunen, M., Krenn, H., Wheeler, S.J., Koskinen, M., Zentar, R., 2005. Effect of anisotropy and destructuration on the behavior of Murro test embankment. Int. J. Geomech. 5 (2), 87–97. http://dx.doi.org/10.1061/(ASCE)1532-3641(2005)5:2(87).

Korff, M., 2013. Response of Piled Buildings to the Construction of Deep Excavations (Doctoral dissertation). University of Cambridge, pp. 1–344. http://dx.doi.org/10.3233/978-1-61499-274-5-i.

Korff, M., Mair, R.J., Van Tol, F.A.F., 2016. Pile-soil interaction and settlement effects induced by deep excavations. J. Geotech. Geoenvironmental Eng. 142 (8), 04016034. http://dx.doi.org/10.1061/(ASCE)GT.1943-5606.0001434.

Lee, C.J., Chen, C.R., 2003. Negative skin friction on piles due to lowering of ground water table. Geotech. Eng. 34 (1), 13–24.

Liang, R., Yin, Z.Y., Yin, J.H., Wu, P.C., 2023. Numerical analysis of time-dependent negative skin friction on pile in soft soils. Comput. Geotech. 155 (October 2022), 105218. http://dx.doi.org/10.1016/j.compgeo.2022.105218.

Lizárraga, J.J., Buscarnera, G., 2020. A geospatial model for the analysis of time-dependent land subsidence induced by reservoir depletion. Int. J. Rock Mech. Min. Sci. 129 (February), http://dx.doi.org/10.1016/j.ijrmms.2020.104272.

Mair, R.J., Taylor, R., Burland, J.B., 1996. Prediction of ground movements and assessment of risk of building damage due to bored tunnelling. In: Mair, R.J., Taylor, R. (Eds.), Geotechnical Aspects of Underground Construction in Soft Ground. Balkema, London, pp. 713–718.

Merisalu, J., Sundell, J., Rosén, L., 2023. Probabilistic cost-benefit analysis for mitigating hydrogeological risks in underground construction. Tunn. Undergr. Space Technol. 131 (October 2022), http://dx.doi.org/10.1016/j.tust.2022.104815.

Ottolini, M., Dijkstra, J., van Tol, F., 2015. Immediate and long-term installation effects adjacent to an open-ended pile in a layered clay. Can. Geotech. J. 52 (7), 982–991. http://dx.doi.org/10.1139/cgj-2014-0222.

Phien-wej, N., Giao, P.H., Nutalaya, P., 2006. Land subsidence in Bangkok, Thailand. Eng. Geol. 82 (4), 187–201. http://dx.doi.org/10.1016/j.enggeo.2005.10.004.

Potts, D.M., Addenbrooke, T.I., 1997. A structure's influence on tunnelling-induced ground movements. Proc. Inst. Civ. Eng. - Geotech. Eng. 125 (2), 109–125. http://dx.doi.org/10.1680/igeng.1997.29233.

Prosperi, A., Longo, M., Korswagen, P.A., Korff, M., Rots, J.G., 2023. Sensitivity modelling with objective damage assessment of unreinforced masonry façades undergoing different subsidence settlement patterns. Eng. Struct. 286 (April), 116113. http://dx.doi.org/10.1016/j.engstruct.2023.116113.

Rankin, W.J., 1988. Ground movements resulting from urban tunnelling: predictions and effects. In: Bell, F.G., Culshaw, M.G., Cripps, J.C., Lovell, M.A. (Eds.), Engineering Geology of Underground Movements, Geological Society Engineering Geology Special Publication. Vol. 5, pp. 79–92. http://dx.doi.org/10.1144/GSL.ENG.1988.005.01.06.

Rodríguez-Rebolledo, J.F., Auvinet-Guichard, G.Y., Martínez-Carvajal, H.E., 2015. Settlement analysis of friction piles in consolidating soft soils. DYNA (Colombia) 82 (192), 211–220. http://dx.doi.org/10.15446/dyna.v82n192.47752.

Shen, S.-L., Xu, Y.-S., 2011. Numerical evaluation of land subsidence induced by groundwater pumping in Shanghai. Can. Geotech. J. 48 (9), 1378–1392. http://dx.doi.org/10.1139/t11-049.

Sundell, J., Haaf, E., Tornborg, J., Rosén, L., 2019. Comprehensive risk assessment of groundwater drawdown induced subsidence. Stoch. Environ. Res. Risk Assess. 33 (2), 427–449. http://dx.doi.org/10.1007/s00477-018-01647-x.

Teatini, P., Ferronato, M., Gambolati, G., Gonella, M., 2006. Groundwater pumping and land subsidence in the Emilia-Romagna coastland, Italy: Modeling the past occurrence and the future trend. Water Resour. Res. 42 (1), 1–19. http://dx.doi.org/10.1029/2005WR004242.

Tomlinson, M.J., 1957. The adhesion of piles driven in clay soils. In: Proceedings of the 4th International Conference on Soil Mechanics and Foundation Engineering. Vol. 2, Butterworths Scientific Publications, London, pp. 66–71.

Tornborg, J., Karlsson, M., Dijkstra, J., 2024. Temporal effective stress response of soil elements below the base of an excavation in sensitive clay. Can. Geotech. J. 61 (11), 2571–2587. http://dx.doi.org/10.1139/cgj-2023-0355.

Tornborg, J., Karlsson, M., Karstunen, M., 2023. Permanent sheet pile wall in soft sensitive clay. J. Geotech. Geoenvironmental Eng. 149 (6), 1–13. http://dx.doi.org/10.1061/jggefk.gteng-10955.

Tornborg, J., Karlsson, M., Kullingsjö, A., Karstunen, M., 2021. Modelling the construction and long-term response of Göta Tunnel. Comput. Geotech. 134 (March), 104027. http://dx.doi.org/10.1016/j.compgeo.2021.104027.

Van Langen, H., Vermeer, P.A., 1990. Automatic step size correction for non-associated plasticity problems. 29, 579–598. http://dx.doi.org/10.1002/nme.1620290308.

Van Langen, H., Vermeer, P.A., 1991. Interface elements for singular plasticity points. Int. J. Numer. Anal. Methods Geomech. 15 (5), 301–315. http://dx.doi.org/10.1002/nag.1610150502.

Vermeer, P.A., Neher, H.P., 1999. A soft soil model that accounts for creep. In: Beyond 2000 in Computational Geotechnics. Ten Years of PLAXIS International. Proceedings of the International Symposium, Amsterdam, March 1999. pp. 249–261. http://dx.doi.org/10.1201/9781315138206-24.

Wang, R., Brandenberg, S.J., 2013. Beam on nonlinear Winkler foundation and modified neutral plane solution for calculating downdrag settlement. J. Geotech. Geoenvironmental Eng. 139 (9), 1433–1442. http://dx.doi.org/10.1061/(asce)gt.1943-5606.0000888.

Wheeler, S.J., Näätänen, A., Karstunen, M., Lojander, M., 2003. An anisotropic elastoplastic model for soft clays. Can. Geotech. J. 40 (2), 403–418. http://dx.doi.org/10.1139/t02-119.

Wikby, P., Abed, A., Karlsson, M., Sundell, J., Karstunen, M., 2023. The influence of parameter variability on subsidence. In: Zdravkovic, L., Kontoe, S., Taborda, D., Tsiampousi, A. (Eds.), Proceedings of the 10th European Conference on Numerical Methods in Geotechnical Engineering. International Society for Soil Mechanics and Geotechnical Engineering, pp. 1–6. http://dx.doi.org/10.53243/NUMGE2023-325.

Wikby, P., Haaf, E., Abed, A., Rosén, L., Sundell, J., Karstunen, M., 2024. A grid-based methodology for the assessment of time-dependent building damage at large scale. Tunn. Undergr. Space Technol. 149, 105788. http://dx.doi.org/10.1016/j.tust.2024.105788.

Ye, S., Xue, Y., Wu, J., Yan, X., Yu, J., 2016. Progression and mitigation of land subsidence in China. Hydrogeol. J. 24 (3), 685–693. http://dx.doi.org/10.1007/s10040-015-1356-9.

Zhang, X., Liu, X., Chang, Z., Liu, Z., Yu, D., Li, Y., 2022. Time dependence of neutral plane position in a PHC-supported soft subgrade. J. Geotech. Geoenvironmental Eng. 148 (2), 1–13. http://dx.doi.org/10.1061/(ASCE)GT.1943-5606.0002748.

Zhang, G., Wu, Y., Wang, L., Zhang, K., Daemen, J.J., Liu, W., 2015. Time-dependent subsidence prediction model and influence factor analysis for underground gas storages in bedded salt formations. Eng. Geol. 187, 156–169. http://dx.doi.org/10.1016/j.enggeo.2015.01.003.